

**SHAPE-CONTROLLED SYNTHESIS OF SILVER NANO-  
PARTICLES MEDIATED BY DNA AND THEIR  
ANTIBACTERIAL AND ANTIOXIDANT  
ACTIVITIES**



**A Thesis Submitted in Partial Fulfillment of the Requirements for the  
Degree of Master of Science in Environmental Biology**

**Suranaree University of Technology**

**Academic Year 2018**

การสังเคราะห์อนุภาคนาโนซิลเวอร์แบบควบคุมรูปร่างโดยใช้ดีเอ็นเอและ  
การศึกษาฤทธิ์ต้านแบคทีเรียและฤทธิ์ต้านอนุมูลอิสระ

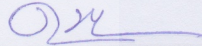


วิทยานิพนธ์นี้เป็นส่วนหนึ่งของการศึกษาตามหลักสูตรปริญญาวิทยาศาสตรมหาบัณฑิต  
สาขาวิชาชีววิทยาสิ่งแวดล้อม  
มหาวิทยาลัยเทคโนโลยีสุรนารี  
ปีการศึกษา 2561

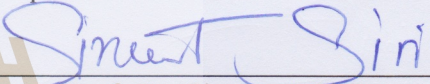
**SHAPE-CONTROLLED SYNTHESIS OF SILVERNANO-  
PARTICLES MEDIATED BY DNA AND THEIR  
ANTIBACTERIAL AND ANTIOXIDANT ACTIVITIES**

Suranaree University of Technology has approved this thesis submitted in partial fulfillment of the requirements for a Master's Degree.

Thesis Examining Committee

  
\_\_\_\_\_  
(Asst. Prof. Dr. Duangkamol Maensiri)

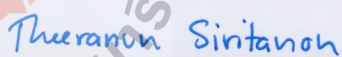
Chairperson

  
\_\_\_\_\_  
(Assoc. Prof. Dr. Sineenat Siri)

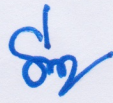
Member (Thesis Advisor)

  
\_\_\_\_\_  
(Dr. Pongrit Krubphachaya)

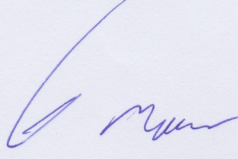
Member

  
\_\_\_\_\_  
(Asst. Prof. Dr. Theeranun Siritanon)

Member

  
\_\_\_\_\_  
(Prof. Dr. Santi Maensiri)

Vice Rector for Academic Affairs  
and Internationalization

  
\_\_\_\_\_  
(Asst. Prof. Dr. Worawat Meevasana)

Dean of Institute of Science

นวพร ศรีทอง : การสังเคราะห์อนุภาคนาโนซิลเวอร์แบบควบคุมรูปร่างโดยใช้ดีเอ็นเอและการศึกษาฤทธิ์ต้านแบคทีเรียและฤทธิ์ต้านอนุมูลอิสระ (SHAPE-CONTROLLED SYNTHESIS OF SILVER NANOPARTICLES MEDIATED BY DNA AND THEIR ANTIBACTERIAL AND ANTIOXIDANT ACTIVITIES). อาจารย์ที่ปรึกษา : รองศาสตราจารย์ ดร.สินีนานู ศรี, 80 หน้า.

เนื่องด้วยมีความต้องการอนุภาคนาโนซิลเวอร์รูปร่างต่าง ๆ และการตระหนักถึงผลกระทบของการผลิตเชิงสิ่งแวดล้อม งานวิจัยนี้จึงศึกษาถึงการสังเคราะห์อนุภาคนาโนซิลเวอร์รูปร่างต่าง ๆ แบบเป็นมิตรต่อสิ่งแวดล้อม โดยการสังเคราะห์อนุภาคนาโนซิลเวอร์ถูกควบคุมโดยดีเอ็นเอชนิดต่าง ๆ (ดีเอ็นเอสายสั้น A30 และ C30) และดีเอ็นเอสายยาว (พลาสมิดดีเอ็นเอ pGADT7 8.0 กิโลเบส) และไดโอดเปล่งแสงที่มีความยาวคลื่นต่าง ๆ (460 520 และ 620 นาโนเมตร) ผลการศึกษาแสดงให้เห็นว่า ปริมาณดีเอ็นเอ ความยาวดีเอ็นเอ อัตราส่วนโดยโมลาร์ของซิลเวอร์ไนเตรทและดีเอ็นเอ ความยาวคลื่นของไดโอดเปล่งแสง และระยะเวลาของปฏิกิริยา เป็นปัจจัยสำคัญในการเปลี่ยนแปลงรูปร่างของอนุภาคนาโนซิลเวอร์รูปร่างกลมไปเป็นรูปร่างอื่น การสังเคราะห์อนุภาคนาโนซิลเวอร์โดยใช้พลาสมิดดีเอ็นเอเป็นสารคงทำให้คงตัว พบว่าได้อนุภาคนาโนซิลเวอร์แบบคอลลอยด์สี่เหลี่ยม สี่เหลี่ยม และเตี้ย ซึ่งขึ้นอยู่กับปริมาณดีเอ็นเอและความยาวคลื่นแสงที่ได้รับ โดยอนุภาคนาโนซิลเวอร์คอลลอยด์สี่เหลี่ยม นอกจากประกอบด้วยอนุภาครูปร่างทรงกลม ( $12.32 \pm 2.22$  นาโนเมตร) แล้ว ยังพบรูปร่างหกเหลี่ยม ( $23.03 \pm 6.62$  นาโนเมตร) และสามเหลี่ยมมุมตัด ( $15.84 \pm 4.31$  นาโนเมตร) สำหรับปฏิกิริยาที่ใช้ดีเอ็นเอ C30 ได้ผลคล้ายกับการใช้พลาสมิดดีเอ็นเอคือ ได้อนุภาคนาโนซิลเวอร์แบบคอลลอยด์สี่เหลี่ยมซึ่งประกอบด้วยอนุภาครูปร่างทรงกลม หกเหลี่ยมมุมตัด แบบยาว และสามเหลี่ยมมุมตัด ซึ่งมีขนาดเส้นผ่านศูนย์กลางเฉลี่ย  $24.38 \pm 6.02$  นาโนเมตร ในทางตรงกันข้ามดีเอ็นเอ A30 ช่วยในการเกิดอนุภาคนาโนซิลเวอร์รูปร่างทรงกลมเป็นส่วนใหญ่ ( $26.53 \pm 6.96$  นาโนเมตร) และได้คอลลอยด์สี่เหลี่ยม จากการวิเคราะห์อนุภาคนาโนซิลเวอร์ที่ผลิตได้ด้วยเทคนิค X-ray diffraction selected area electron diffraction และ high resolution transmission electron microscopy บ่งบอกถึงโครงสร้างผลึกของอนุภาคนาโนซิลเวอร์ที่ได้เป็นแบบ face-centered cubic ทั้งนี้อนุภาคนาโนซิลเวอร์ที่สังเคราะห์ขึ้นมีฤทธิ์ต้านอนุมูลอิสระที่ใกล้เคียงกัน

สำหรับการต้านแบคทีเรีย พบว่าอนุภาคนาโนซิลเวอร์ที่หุ้มด้วยพลาสมิดดีเอ็นเอแสดงฤทธิ์ต้านแบคทีเรียได้ดีที่สุดทั้งต่อแบคทีเรีย แกรมลบ *Escherichia coli* และแบคทีเรียแกรมบวก *Staphylococcus aureus* เมื่อเปรียบเทียบกับอนุภาคนาโนซิลเวอร์ที่หุ้มด้วยดีเอ็นเอ A30 และ C30



สาขาวิชาชีววิทยา

ปีการศึกษา 2561

ลายมือชื่อนักศึกษา อนุพร ศรีทอง

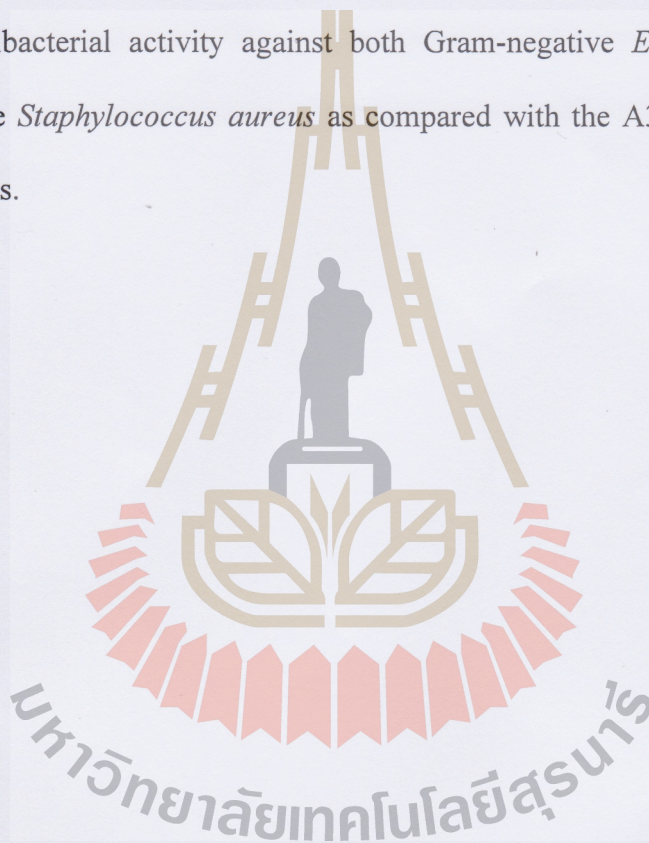
ลายมือชื่ออาจารย์ที่ปรึกษา [Signature]

NAVAPORN SRITONG : SHAPE-CONTROLLED SYNTHESIS OF  
SILVER NANOPARTICLES MEDIATED BY DNA AND THEIR  
ANTIBACTERIAL AND ANTIOXIDANT ACTIVITIES. THESIS  
ADVISOR : ASSOC. PROF. SINEENAT SIRI, Ph.D. 80 PP.

LIGHT EMITTING DIODES/ DNA/ SILVER NANOPARTICLES/ SHAPE  
CONVERSION

With demand of different shapes of silver nanoparticles along with the environmental concern of their production, the eco-friendly syntheses of anisotropic AgNPs were studied in this work. The syntheses of AgNPs were controlled by different types of DNA (short DNA; oligo dA<sub>30</sub> and oligo dC<sub>30</sub>) and long DNA (8.0-kb pGADT7) and different wavelengths (460, 520, and 620 nm) of light emitting diodes (LEDs). The results demonstrated that DNA content, DNA length, molar ratio between AgNO<sub>3</sub> and DNA, LED wavelength, and reaction time played the important roles in a transformation of spherical silver seeds into non-spherical shapes. The synthesized AgNPs using the plasmid DNA as capping agent appeared as yellow, orange, and green colloidal AgNPs depending on DNA content and LED wavelength, and transmission electron microscope (TEM) images revealed their different shapes. The green colloidal AgNPs clearly showed the presence of hexagonal ( $23.03 \pm 6.62$  nm), and corner-truncated triangle ( $15.84 \pm 4.31$  nm) in addition to spherical shapes ( $12.32 \pm 2.22$  nm). Similar to the use of plasmid DNA, the reaction using C30 DNA appeared as green color and contained truncated hexagonal, flat elongated, and truncated triangular shapes in addition to spherical shape with the average size of

$24.38 \pm 6.02$  nm. In contrast, A30 DNA mainly assisted the formation of spherical AgNPs ( $26.53 \pm 6.96$  nm) appearing as deep yellow color. The further analyses of X-ray diffraction, selected area electron diffraction, and high resolution transmission electron microscopy indicated the crystalline nature of all synthesized AgNPs as the face-centered cubic silver. All synthesized AgNPs exhibited similar antioxidant activities. For their antibacterial activity, the plasmid-capped AgNPs exhibited the strongest antibacterial activity against both Gram-negative *Escherichia coli* and Gram-positive *Staphylococcus aureus* as compared with the A30-capped and C30-capped AgNPs.



School of Biology

Academic Year 2018

Student's Signature

นางพร ศิริทอง

Advisor's Signature

## ACKNOWLEDGEMENTS

My master thesis would not have been completed without the great help and support from these kind people.

Firstly, I would like to express my sincere gratitude to my advisor Assoc. Prof. Dr. Sineenat Siri for being my great mentor for 5 years since undergrad year. Because of her inspiration, patience, motivation, and immense knowledge, I can be who I am in the present. She challenged me to initiate a new project that no one in the lab did it before. It was very hard for me at the first place. However, I came across all obstacles and walked in the right direction because of her guidance and help. I have learned not only research skills but also life skill from her. She gave me the great opportunities to have some experiences abroad, i.e. joining conferences and doing short-term research. Moreover, she always encourages me when I faced with discouragement or disappointment.

Besides my advisor, I would like to thanks all teachers, who sharpen my scientific knowledge and staffs, who help me about the paperworks.

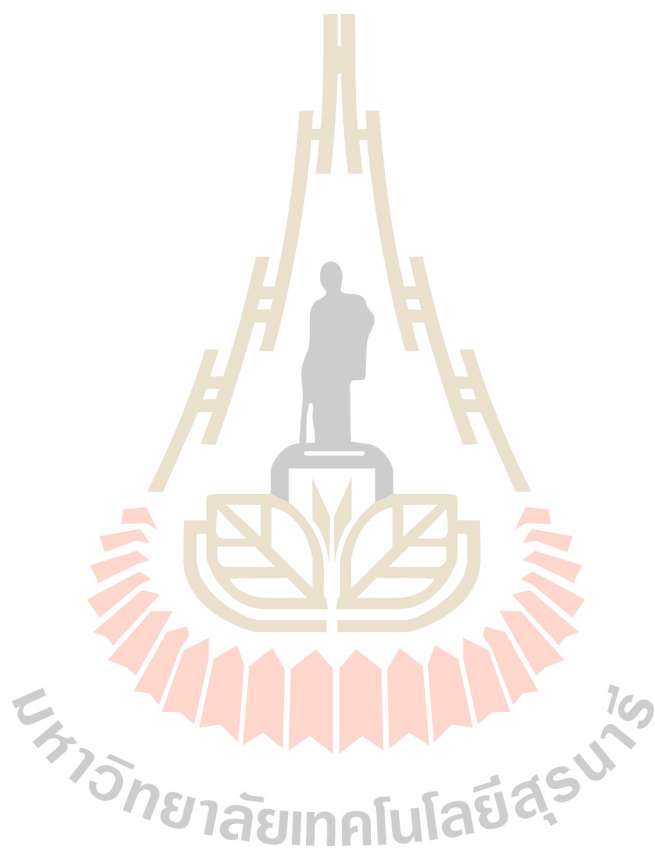
I thank all SIRI lab members for their advices, support, encouragement and for all the fun we have had in the past five years. Also I thank my friends in the first batch of honor program, especially in biology major, who always sharing knowledge, happiness and sadness.

I also would like to thank the Development and Promotion of Science and Technology Talent Project (DPST) for financial support since my bachelor's degree.



Last but not the least, I would like to thank my family: my parents and to my brother for supporting me spiritually throughout writing this thesis and my life in general. Thank for believing in myself and understand the path that I chose.

Navaporn Sritong



# CONTENTS

	<b>Page</b>
ABSTRACT IN THAI.....	I
ABSTRACT IN ENGLISH .....	III
ACKNOWLEDGEMENTS.....	V
CONTENTS.....	VII
LIST OF TABLES.....	X
LIST OF FIGURES .....	XI
<b>CHAPTER</b>	
<b>I INTRODUCTION.....</b>	<b>14</b>
1.1 Background.....	14
1.2 Research objectives.....	17
1.3 Scope of the study.....	17
<b>II LITERATURE REVIEWS.....</b>	<b>19</b>
2.1 Reducing agent.....	19
2.2 Capping agent .....	21
2.3 DNA as a capping agent for synthesizing metal nanoparticles.....	22
2.4 Light-mediated growth of nanoparticles.....	25
2.5 Effect of different shapes on antibacterial and antioxidant activities...	29
<b>III MATERIALS AND METHODS .....</b>	<b>31</b>
3.1 Plasmid DNA extraction and purification.....	31
3.2 Synthesis of AgNPs .....	32

## CONTENTS (Continued)

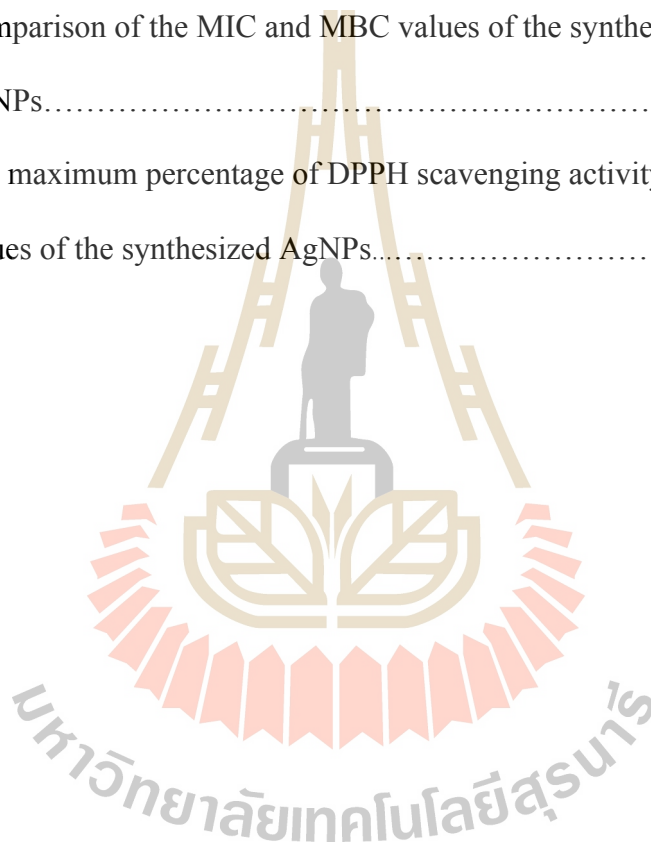
	<b>Page</b>
3.3 Characterization of the synthesized AgNPs .....	33
3.3.1 Morphology and size distribution.....	33
3.3.2 The crystallographic characterization .....	33
3.4 Determination of antioxidant activity of the synthesized AgNPs .....	34
3.5 Determination of antibacterial activity of the synthesized AgNPs .....	34
3.6 Statistical analysis .....	35
<b>IV RESULTS AND DISCUSSION .....</b>	<b>36</b>
4.1 Production of different shaped AgNPs using plasmid DNA.....	36
4.1.1 Plasmid DNA preparation .....	36
4.1.2 Effects of reducing agents and wavelength of LEDs on a formation of AgNPs .....	37
4.1.3 Effects of DNA content on a formation of AgNPs .....	40
4.1.4 Effects of the synthesis time on a formation of AgNPs .....	41
4.1.5 Characterization of the plasmid-capped AgNPs .....	42
4.1.6 Antibacterial activity of the plasmid-capped AgNPs.....	47
4.1.7 Antioxidant activity of the plasmid-capped AgNPs.....	49
4.2 Production of different shaped AgNPs using oligo dA and dC .....	50
4.2.1 Effect of DNA content and synthesis time on a formation of AgNPs using A30.....	50
4.2.2 Effect of DNA content and synthesis time on a formation of AgNPs using C30 .....	52

## CONTENTS (Continued)

	<b>Page</b>
4.2.3 Characterization of the A30-capped and C30-capped AgNPs ...	54
4.2.4 Antibacterial activity of the synthesized AgNPs.....	59
4.3 Comparison of the plasmid-capped, A30-capped, and C30-capped AgNPs .....	62
4.3.1 Morphology, average sizes, and characterization .....	62
4.3.2 Antibacterial activity .....	64
4.3.3 Antioxidant activity.....	65
<b>V CONCLUSION .....</b>	<b>66</b>
REFERENCES .....	68
CURRICULUM VITAE.....	80

## LIST OF TABLES

Table		Page
4.1	Comparison of optimized synthesis condition and morphologies of the synthesized AgNPs.....	64
4.2	Comparison of the MIC and MBC values of the synthesized AgNPs.....	65
4.3	The maximum percentage of DPPH scavenging activity and IC <sub>50</sub> values of the synthesized AgNPs.....	65



## LIST OF FIGURES

Figure	Page
2.1 The adsorption of (A) a repeating unit of PVP and (B) a citrate ion on Ag [100] and Ag [111] surfaces, respectively .....	22
2.2 The sites of (A) adenine and (B) cytosine for bonding with AgNPs .....	24
2.3 Time-dependent UV-Vis spectra showing the conversion of silver nanospheres to nanoprism.....	26
2.4 UV/vis spectral changes as the Ag seeds were exposed to LED irradiation at (A) 455, (B) 627, and (C) 720 nm and TEM images of the correlated final product.....	27
2.5 Time course UV-Vis spectra of AgNP solutions during natural sunlight irradiation and the corresponding photographs of solution colors. The concentrations of citrate in solution were (A) $5 \times 10^{-4}$ , (B) $10^{-3}$ , (C) $2.5 \times 10^{-3}$ , and (D) $5.0 \times 10^{-3}$ .....	28
4.1 The pattern of extracted plasmid DNA from <i>E. coli</i> containing pGADT7-AD visualized on 0.8% agarose gel.....	37
4.2 UV-Vis spectra of the synthesized AgNPs in the reactions using glucose as weak reducing agent and pGADT7 as capping agent .....	38
4.3 UV-Vis spectra of the formed AgNPs under different conditions .....	40
4.4 UV-Vis spectra of the synthesized AgNPs in the reactions containing different amount of pGADT7-AD at 24 h under the blue LED irradiation ...	41

## LIST OF FIGURES (Continued)

Figure	Page
4.5	UV–Vis spectra of the synthesized AgNPs in the reactions containing (A) 4 pmole and (B) 8 pmole of pGADT7-AD in a time course of 24 h under the blue light irradiation..... 42
4.6	Representative TEM images of the plasmid-capped AgNPs in the reactions containing (A) 2 pmole, (B) 4 pmole, and (C) 8 pmole of DNA ... 44
4.7	Characterization of the plasmid-capped AgNPs (4 pmole). (A) XRD pattern, (B) SAED-TEM, and (C) HR-TEM ..... 46
4.8	Growth curves of (A) <i>E. coli</i> and (B) <i>S. aureus</i> in response to different concentrations of the synthesized AgNPs in a time course of 24 h..... 48
4.9	DPPH free radical scavenging activity of the plasmid capped AgNPs and positive control, ascorbic acid..... 50
4.10	UV–Vis spectra of the synthesized AgNPs in the reactions containing different amounts of A30 under the blue light irradiation for 48 h ..... 51
4.11	UV–Vis spectra of the synthesized AgNPs in the reactions containing 16 pmole of A30 under the blue light irradiation in a time course of 48 h ..... 52
4.12	UV–Vis spectra of the synthesized AgNPs in the reactions containing different amounts of C30 under the blue light irradiation for 48 h..... 53

## LIST OF FIGURES (Continued)

Figure	Page
4.13	UV–Vis spectra of the synthesized AgNPs in the reactions containing 16 pmole of C30 under the blue light irradiation in a time course of 48 h.... 54
4.14	Characterization of the A30-capped AgNPs as analyzed by (A) TEM, (B) XRD, and (C) SAED-TEM.....57
4.15	Characterization of the C30-capped AgNPs as analyzed by (A) TEM, (B) XRD, and (C) SAED-TEM ..... 58
4.16	Growth curves of (A) <i>E. coli</i> and (B) <i>S. aureus</i> in response to different concentrations of the A30-capped AgNPs in a time course of 24 h. .... 59
4.17	Growth curves of (A) <i>E. coli</i> and (B) <i>S. aureus</i> in response to different concentrations of the C30-capped AgNPs in a time course of 24 h ..... 60
4.18	DPPH free radical scavenging activity of the A30-capped AgNPs, C30-capped AgNPs, and ascorbic acid (positive control).....61



# CHAPTER I

## INTRODUCTION

### 1.1 Background

According to the excellent and unique properties, silver nanoparticle (AgNP) is one of the most researched metal nanomaterials that has been applied in various fields of applications such as biosensors, chemical catalysts, electronics, photonics, information storages, optoelectronics, antimicrobial agents, antioxidant agents, and anticancer agents (Beyene et al., 2017). Interestingly, the properties of AgNPs greatly depend on their size and shape (Raza et al., 2016), thus the size- and shape-controlled syntheses of AgNPs are the challenge for their production and potential applications. With different shapes, AgNPs offer different properties, which are suitable for various applications. For example, AgNPs with different shapes provide different antibacterial efficiencies for medical applications (Hong et al., 2016; Raza et al., 2016) and different catalytic activities for various chemical reactions (Wiley et al., 2005). Thus, a shape-controlled synthesis is mainly focused in this work. In general, factors affecting the formation of different shapes of AgNPs are the reduction rates, types of capping agents, the molar ratio of reductant and metal precursor, and different wavelengths of light activation (Mansouri and Ghader, 2009; Stamplecoskie and Scaiano, 2010). The synthesis reaction of AgNPs begins with the nucleation or the reduction of silver ions into silver atoms following by the seed formation (Xia et al., 2009). The different structures of formed seeds eventually define the final shapes of

nanoparticles. The formed seeds may be single crystal or single/multiple twinned structures, which depend on reduction rates of the synthesis reaction. When reduction rate is extremely fast, most seeds become single crystal structure. In contrast, when reduction rate is slow, the multiple or single twinned seeds are the majority of products (Haghi et al., 2013a). Since the reduction rates of the synthesis reaction depend on the reducing powers and concentrations of reducing agents (Mansouri and Ghader, 2009), the use of different types of reducing agent such as strong and weak reducing agents can produce different silver seed structures. The capping agent is considered a key factor for controlling final shapes of nanoparticles in the growth step (Zeng et al., 2010). Each type of capping agent selectively binds to different planes of metal surfaces, thereby inducing the formation of metal nanocrystals with different shapes (Xia et al., 2015). The different molar ratios of reductant and metal precursor are another factor controlling the morphologies of the synthesized AgNPs. Rivero and colleagues discovered the synthesis of multicolor silver nanoparticles by tuning reducing agent/silver ion molar ratios. With increasing of molar ratio, the maximum absorbance band is shifted to shorter wavelengths and provides various shades of color (orange, green, and blue) relating to different shapes of synthesized AgNPs (Rivero et al., 2013). The photo-induction process has received the increasing interest as a simple, effective approach to mediate a formation of different-shaped AgNPs (Tang et al., 2015). Several light sources, including fluorescent light, UV light, light emitting diodes (LEDs), laser, and sunlight, were reported to drive the photo-reduction of metal salts and induce the growth of metal seeds into anisotropic shapes (Khamhaengpol and Siri, 2016; Lee et al., 2016; Stampelcoskie and Scaiano, 2010; Tang et al., 2015; Verma et al., 2017; Zheng et al., 2007). The shape conversion direction of AgNPs was

proposed to greatly depend on the excitation wavelength of a specific plasmon. Stampelcoskie and colleagues reported that the 3-nm citrate-capped seeds of AgNPs were transformed into the larger spheres, dodecahedra, triangular plates, and nanorods via the exposure to LED irradiation at 405, 455, 627, and 720 nm, respectively (Stampelcoskie and Scaiano, 2010). Under the exposure to LED irradiation at 520 and 562 nm, the citrate capped seeds of AgNPs were also reported to transfigure to triangular prism and circular plate, respectively (Krajczewski et al., 2014). Alternatively, the citrate-capped seeds of AgNPs were reported for a conversion to nanoprisms by LED activation in a range of 467–630 nm (Saade and de Araújo, 2014)

In addition to a controlled shape, the synthesis of AgNPs with an eco-friendly process is another challenge since the issue of environmental impact on production of AgNPs and other metal nanoparticles are increasingly concerned. Therefore, the production of AgNPs by green technology has gained much research interest. In green syntheses of AgNPs, most works focus on the extract from various species and part of plants (Ahmed et al., 2017; Osibe et al., 2017; Singh et al., 2017), which phytochemicals in plant extracts such as terpenoids, flavones, ketones, aldehydes, amides and carboxylic acids were proposed to function to reduce  $\text{Ag}^+$  to  $\text{Ag}^0$ , while complex carbohydrates stabilized the produced AgNPs (Upadhyay and Verma, 2015). According to reviewed literatures, very few works reported on the use of DNA for the green synthesis of AgNPs. Herring sperm and salmon milt DNA, for examples, were reported to facilitate a formation of spherical AgNPs under an alkaline pH with a strong reducing agent, sodium borohydride (Nithyaja et al., 2012). Recently, the use of bacterial genomic DNA for assisting a formation of spherical AgNPs via a green synthesis approach without the use of alkaline solution was reported (Chumpol and

Siri, 2017). Nevertheless, the green synthesis of non-spherical AgNPs mediated by DNA molecules under a neutral condition is still a challenge. Thus, this work is interesting to investigate on the use of small size DNA, a plasmid DNA, for assisting a green production of non-spherical AgNPs via the LED-irradiation activation. Moreover, the antibacterial and antioxidant activities of the different-shaped AgNPs were investigated.

## 1.2 Research objectives

1.2.1 To synthesize different shaped AgNPs by controlling three factors: reducing agents ( $\text{NaBH}_4$  and glucose), capping agents (Oligo dA, Oligo dC, and plasmid DNA), and wavelengths of LEDs (460 nm, 520 nm, and 620 nm.)

1.2.2 To characterize the synthesized AgNPs.

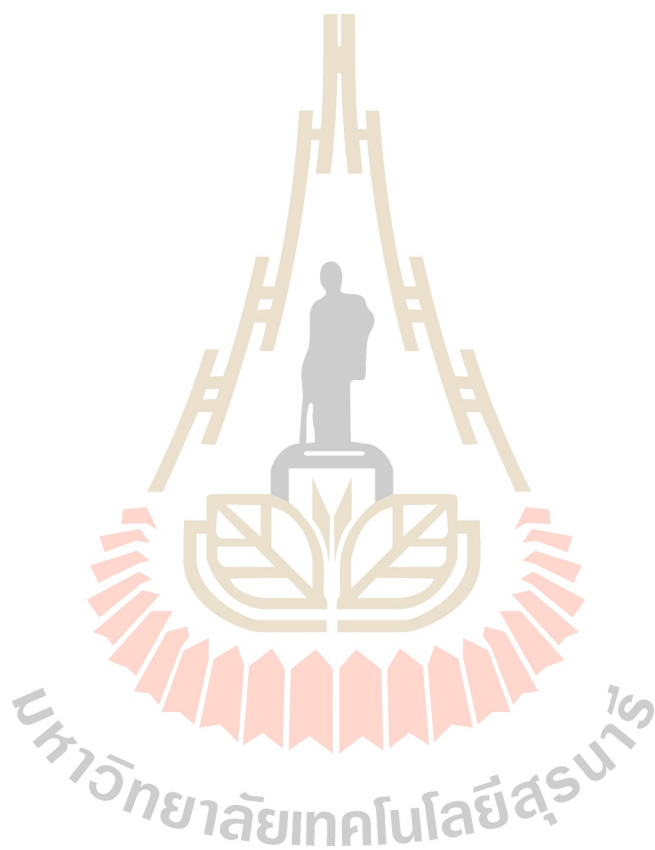
1.2.3 To study the antioxidant activity of the synthesized AgNPs.

1.2.4 To study the antibacterial activity of the synthesized AgNPs.

## 1.3 Scope of the study

This research is divided into 3 parts, which are the optimization of synthesized conditions, characterization of the synthesized AgNPs, and determination of the antioxidant and antibacterial activities of the produced nanoparticles. The reducing agent used in this work included strong reducing agent ( $\text{NaBH}_4$ ) and weak reducing agent (glucose). For the capping agent, two different short DNA primers (oligo dA<sub>30</sub> (A30) and oligo dC<sub>30</sub> (C30)) and long DNA (8.0-kb pGADT7) were employed.

In the growth step of nanoparticles, the high power LED with various wavelengths (460 nm, 520 nm, and 620 nm.) is used to transform silver seed into various final shapes.



## CHAPTER II

### LITERATURE REVIEWS

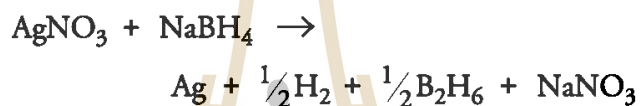
Generally, a typical synthesis of metal nanoparticles is divided into three distinct stages: 1) nucleation, 2) evolution of nuclei into seeds, and 3) growth of seeds into nanocrystals (Xia et al., 2009). The step at which  $\text{Ag}^+$  ions are reduced to  $\text{Ag}^0$  followed by agglomeration into a small cluster (nuclei) called nucleation. After this step, the evolution of nuclei into seeds takes place and resulted in different seed structures. Finally, well-defined nanocrystals growing from each seed structure are formed. Thus, a possible method to achieve controlled-shape AgNPs is to control one or more of these steps.

#### 2.1 Reducing agent

The reducing agent is considered as a factor influencing the growth of AgNPs into different sizes and morphologies in the steps of nucleation and seed formation (Troupis et al., 2008). The reducing power of each reducing agent affects the rate of reduction (nucleation step) and finally influences the final shape of nanoparticles. The use of strong reducing agents results in a fast reduction rate, resulting in the production of the small particle seeds in single crystal structure with uniform size distribution (Haghi et al., 2013b; Mansouri and Ghader, 2009). Conversely, weak reducing agents require a longer time to complete the reduction process. As a consequence of the slow rate, this reaction contains larger nanoseeds (Pacioni et al., 2015) and the majorities

of the products are the multiple or single twinned seeds. Since the use of various silver seed nanoparticles leads to a formation of significantly different nanostructures (Krajczewski et al., 2015), different reducing agents can be used as a factor to control the obtained seed structure and eventually different final shape of AgNPs.

Sodium borohydride ( $\text{NaBH}_4$ ) is a strong reducing agent that has been used in many chemical approaches in order to produce small particle seeds (Lu and Chou, 2008; Mansouri and Ghader, 2009). The reduction of  $\text{AgNO}_3$  by  $\text{NaBH}_4$  is shown as the following chemical equation (Mulfinger et al., 2007a):



From this chemical reduction, the yellow colloidal silver seeds can be obtained within three minutes. Moreover, the synthesized silver seeds are in spherical shape with a diameter of approximately 12 nm and show the surface plasmon resonance (SPR) peak of silver near 400 nm (Mulfinger et al., 2007a).

The weak reducing agents like trisodium citrate and glucose require high temperature and adjusted pH aside from longer time to complete the reduction process (Mansouri and Ghader, 2009). In the case of glucose, the reducing sugar, the temperature above 60 °C or pH 11 is needed to produce gluconic acid that acts as a reductant in the reaction. The gluconic acid has abundant hydroxyl groups that can reduce  $\text{Ag}^+$  ions to elemental silver. In addition to its reducing function, the oxidation of hydroxyl groups of gluconic acid to carboxyl groups also occurs. As a result, the negative charges of the carboxyl groups can stabilize AgNPs (Amany et al., 2012; Ortega-Arroyo et al., 2013).

## 2.2 Capping agent

The capping agent is one of the important components in the synthesis of nanoparticles since they prevent further aggregation of nanoparticles and consequently, prolong the stability of the synthesized nanoparticles. Aside from mentioned functions, capping agents are proved as a crucial factor for controlling final shapes of nanoparticles (Zeng et al., 2010). The mechanism behind this role is that each capping agent has a different binding affinity toward different facets of nanocrystals leading to an unequal growth rate of metal atom on each crystal facet (Ajitha et al., 2016) and thereby induce the formation of metal nanocrystals with different shapes (Xia et al., 2015).

Polyvinyl pyrrolidone (PVP) and sodium citrate are the common capping agents for a synthesis of AgNPs. These two capping agents bind strongly to different planes of nanocrystals (Figure 2.1). In a case of single-crystal seeds, which terminated with only [111] and [100] facets, PVP preferentially binds to [100] facets of AgNPs and hinders the growth rate of this facet. Thus, Ag atoms will preferentially add to the [111] facets, resulting in an elongation of the [100] facets and the formation of [100]-enclosed nanocubes. In contrast, citrate has been shown to bind more strongly to [111] than [100] facets, favoring the formation of nanoplates enclosed by a large portion of [111] facets (Xia et al., 2009; Zeng et al., 2010).



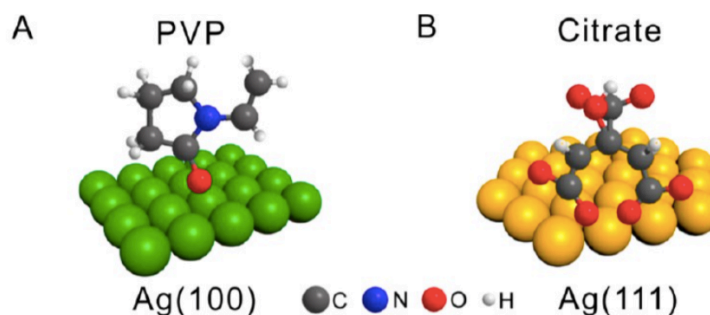


**Figure 2.1** The adsorption of (A) a repeating unit of PVP and (B) a citrate ion on Ag [100] and Ag [111] surfaces, respectively (Xia et al., 2015).

### 2.3 DNA as a capping agent for synthesizing metal nanoparticles

In addition to chemical capping agents, biomolecules can be employed as capping agents because they contain functional groups that selectively bind to particular surfaces of metal nanoparticles (Xia et al., 2015).

Among these biological molecules, DNA is one of the abundant molecules that are potentially used for mediating a formation of AgNPs via a green synthesis approach but very few works were reported. The plasmid DNA with an average size of 3,980 base pairs extracted from *Bacillus* was acted as both capping and reducing agents in the photoinduced synthesis of AgNPs (Zhang et al., 2011). Herring sperm and salmon milt DNA were also reported to mediate a formation of AgNPs in the condition with  $\text{NaBH}_4$  and in alkaline pH (Nithyaja et al., 2012; Zhang et al., 2011). In addition, a recent research in the use of bacterial genomic DNA for assisting a formation of AgNPs via a green synthesis approach without the use of alkaline solution was reported (Chumpol and Siri, 2017). However, all of mentioned reports of using DNA for green synthesis of AgNPs could produce AgNPs only in a spherical or shape. sis of gold nanoparticles with controllable morphology (Tan et al., 2014). Wang

and his colleagues discovered that the short DNA sequence with 30 similar bases (oligo dA, oligo dC, oligo dG and oligo dT) could govern the growth of Au seed into various morphologies. Moreover, the results from their work also revealed that different structures of Au seed resulted in different final shapes of gold nanoparticles (Wang et al., 2012; Wang et al., 2010).

In 2016, Farkhari and colleagues published the research work that clearly showed the functional groups responsible for bonding between N-bases and nanoparticles. As shown in Figure 2.2, the bond between adenine and the nanoparticle takes place at nitrogens of N<sub>1</sub>, N<sub>3</sub>, and N<sub>7</sub>. For cytosine, the oxygen of the main ring N<sub>3</sub> and N<sub>1</sub> is responsible for the interaction with Ag and Au nanoparticles. In the same manner as cytosine, nitrogen atoms in the location N<sub>3</sub> and N<sub>7</sub> together with the oxygen of the main ring of guanine have the most potential for bonding with the nanoparticles. In a case of thymine, there are only two oxygen atoms in the bonds of C=O, which are the potential locations for bonding with the nanoparticles (Farkhari et al., 2016).

However, the utilization of homobase sequences of primers and long base sequences of DNA for controlling the shape of AgNPs is still lacking and this research gap needs to be bridged. From this information, the model of the short homobase sequence was proposed, which possible atoms interacting with the nanoparticle surfaces are indicated in Figure 2.2. Considering from Figure 2.2, oligo dA and oligo dC probably selectively bind to different planes of AgNPs similar to citrate and PVP, respectively.

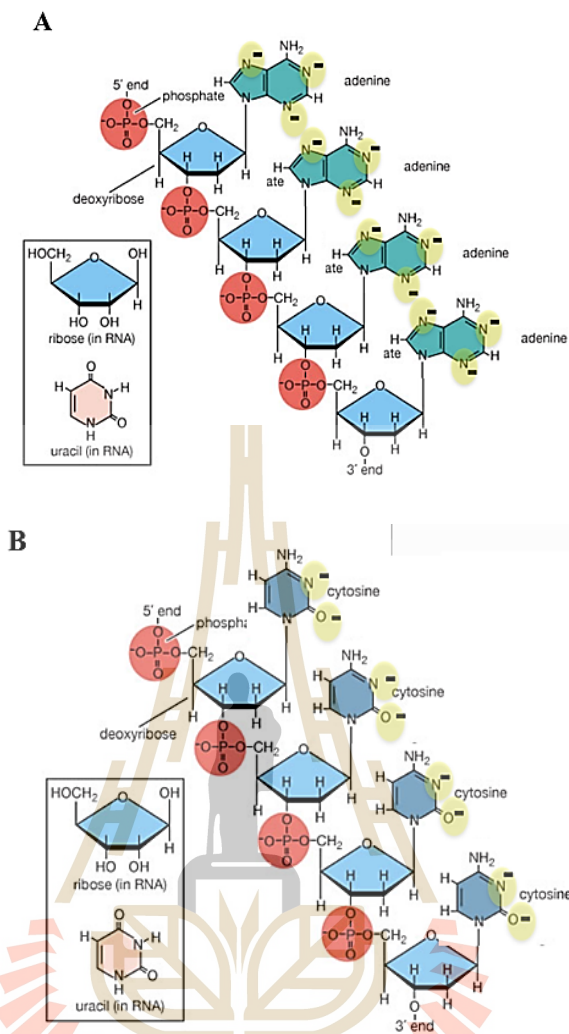


**Figure 2.2** The sites of (A) adenine and (B) cytosine for bonding with AgNPs (<https://www.britannica.com/science/nucleic-acid>).

## 2.4 Light-mediated growth of nanoparticles

A photochemical method is one of the most effective approaches to construct multi-shapes of nanostructure, for example, silver nanowires, nanorods, dodecahedra, bipyramids, triangular nanoplates, and hexagonal (Krajczewski et al., 2015). In this method, various light sources were introduced in growth step in order to drive the growth of the prepared seed nanoparticles that were capped by specific capping agents (Verma et al., 2017). The examples of reported light sources that could serve as potential light sources for the shape transformation of spherical Ag seeds to other shapes are fluorescent light (Jin et al., 2001), laser (Zheng et al., 2007), light emitting diodes (LEDs) (Stamplecoskie and Scaiano, 2010), white light (Krajczewski et al., 2014), and sunlight (Tang et al., 2015).

The first report on the light induced shape transformation of nanoprism AgNPs from spherical Ag seeds was proposed by Mirkin's research group (Jin et al., 2001). The factors that affected the conversion of spherical seeds stabilized by Bis (p-sulfonatophenyl) phenylphosphine dihydrate dipotassium (BSPP) were silver salt precursor and its concentration, the ligand ratio of BSPP to citrate, and wavelength of light. The results showed that the shape conversion of spherical to nanoprism AgNPs could be selectively turned on or off simply by controlling the exposure of the colloid to the light at the appropriate wavelengths, which were 350 to 700 nm. The shape conversion could be observed by the change of color from yellow to green or blue colors depending on sizes and the decrease intensity of the characteristic SPR peak of the spherical AgNPs together with the emergence of the new peak in the range of 470 to 670 nm (Figure 2.3).

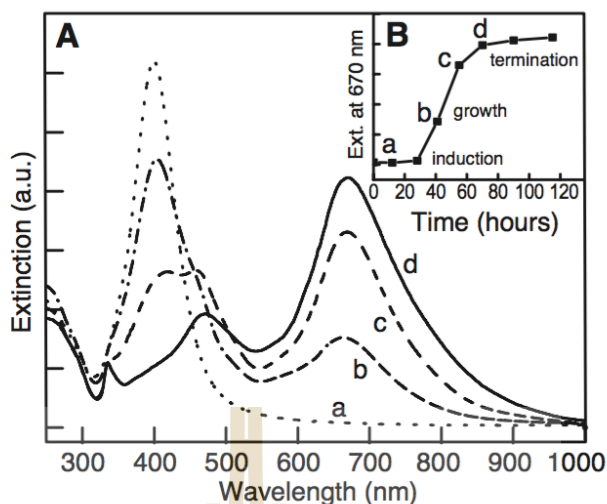


**Figure 2.3** Time-dependent UV-Vis spectra showing the conversion of silver nanospheres to nanoprisms (Jin et al., 2001).

Zheng and coworkers succeeded in the production of monodispersed AgNPs, which their sizes and shapes could be controlled by illuminating silver seeds with specific laser wavelengths (Zheng et al., 2007). Their results revealed the linear relationship between the surface plasmon resonance (SPR) absorption band of the prepared nanoparticles and the excitation wavelengths, in another word, a newly emerged absorption band of products corresponding to the excited wavelength of the given laser, which in turn correlated to color and final morphology of the nanoparticles. The final size and shape were found to depend on the laser wavelength and power. For the exposure to excitation wavelength of 455, 501, and 514 nm, the majorities of products were the mix of disc and triangle nanoparticles, while the laser exposure at 457.9 and 476.5 nm produced the pyramid/pentagon shaped nanoparticles as the main products. The SPR properties of the prepared nanoparticles were finely adjusted in the range of 480 to 560 nm.

In addition to the laser-induced growth of nanoparticles, another photo-transformation of silver nanoparticle model was proposed by Stamplecoskie and Scaiano (Stamplecoskie and Scaiano, 2010). In their work, the silver seeds prepared by the reduction of silver nitrate by I-2959 in the presence of citrate were exposed to various excitation wavelengths of LEDs. The results of this work showed that the 455-nm, 626-nm and 720-nm LEDs controlled the growth of small spherical silver seeds into dodecahedra, nanoplates, and nanorods, respectively. The color change of yellow colloidal and the decrease intensity of SPR peak attributed to the spherical AgNPs together with the emergence of new SPR peak were the evidence of the light-induced shape transformation (Figure 2.4). Apart from the excitation wavelength of light source, the intensity, exposure time, and constant irradiation needed to be considered in order to achieve light-induced growth of nanoparticles with the desired morphology (Pietrobon and Kitaev, 2008).

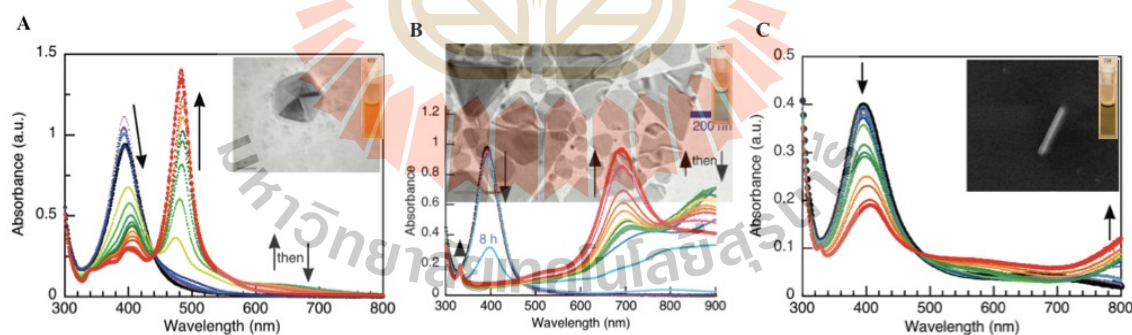


**Figure 2.4** UV/vis spectral changes as the Ag seeds were exposed to LED irradiation at (A) 455, (B) 627, and (C) 720 nm and TEM images of the correlated final products (Stamplecoskie and Scaiano, 2010).

Natural and simulated sunlight were reported to drive the transformation of silver seeds to nanoprism and nanodecahedron depending on the concentration of capping agent, trisodium citrate. At low concentration of citrate, the nanoprisms dominated in the products, whereas the condition with high concentration of citrate gave rise to the decahedron as the major product. New SPR peaks of the solutions with different concentrations of citrate appeared and the color of silver seeds was changed after the silver seed solutions were irradiated for 3 h, which indicates that the anisotropic silver nanoparticles were produced during the irradiation by sunlight (Figure 2.5). In addition, it was found that the UV light from sunlight played an important role in a shape conversion.

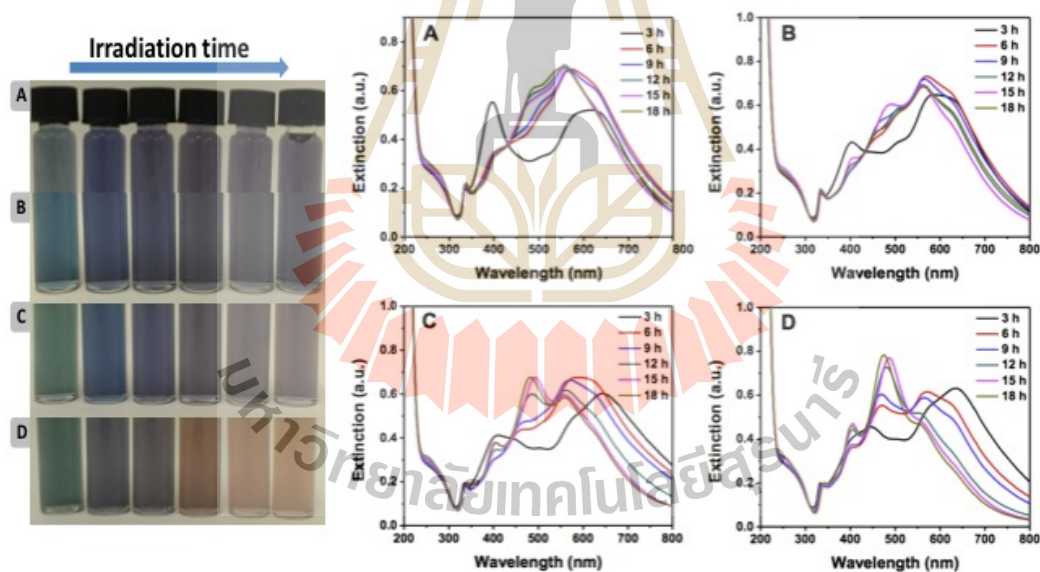


**Figure 2.5** Time course UV-Vis spectra of AgNP solutions during natural sunlight irradiation and the corresponding photographs of solution colors. The concentrations of citrate in solution were (A)  $5 \times 10^{-4}$ , (B)  $10^{-3}$ , (C)  $2.5 \times 10^{-3}$ , and (D)  $5.0 \times 10^{-3}$  Molar (Tang et al., 2015).

Among different light sources, LEDs were found to be one of the cost-effective sources that could generate the controllable shapes of AgNPs with homogeneity and good spectral quality (narrow linewidth) by changing their wavelength and intensity as seen from the results in Figure 2.4 (Stamplecoskie and Scaiano, 2010). Therefore, LEDs were used in this study

## **2.5 Effect of different shapes on antibacterial and antioxidant activities**

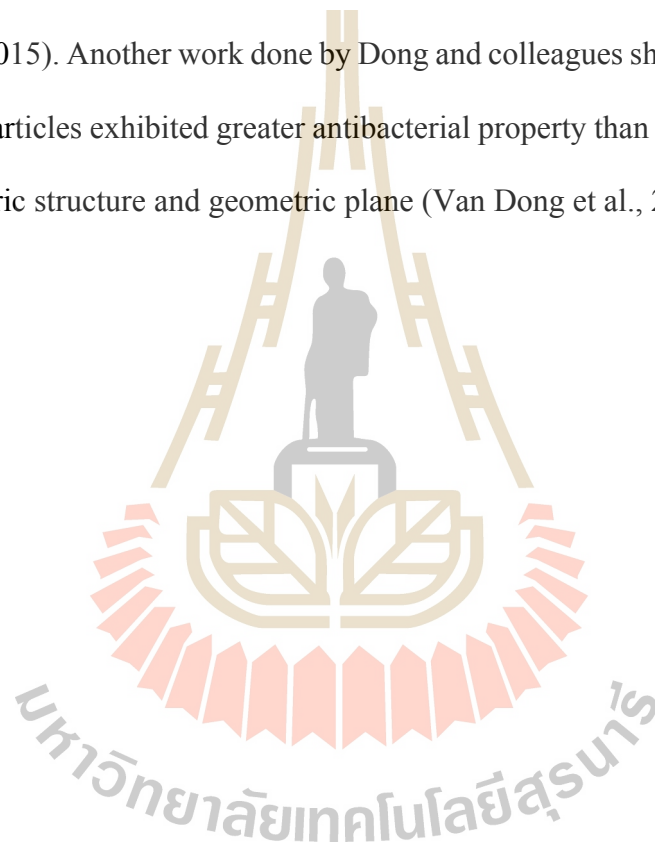
Silver nanoparticles have been used as an effective antimicrobial agent for a long time due to their broad-spectrum antimicrobial property. (Hong et al., 2016). Even though the well-understood mechanism is still ongoing investigated, several possible mechanisms have been proposed. According to their small size, AgNPs may penetrate through the bacterial cell wall and release silver ions into the bacterial cells. These ions may bind to biological macromolecules such as

DNA, proteins, and enzymes. Consequently, it may interfere with DNA replication, protein denaturation, and activity of enzymes (Guzman et al., 2012; Raza et al., 2016).

From a number of previous works on the antibacterial efficacy of AgNPs, it was found that the shape and size of AgNPs play a key role in the antibacterial property (Hong et al., 2016; Nateghi and Hajimirzababa, 2014; Roy et al., 2015). Morones and colleagues reported that the AgNPs with the higher intensity of [111] facet having the higher atom density and higher reactivity than the other facets were more likely to attach to bacterial cell membrane and enhance the bacterial killing efficiency (Morones et al., 2005). Moreover, the AgNPs with more reactive facets showed the



increased rate of silver ion releasing, leading to an enhancement of antibacterial efficacy (Hong et al., 2016). This work was supported by several research works. For example, Roy and colleague reported the antibacterial activity of four different shapes (spherical, oval, rod, and flower shape) of AgNPs against Gram-negative and Gram-positive bacteria, which the flower shaped AgNPs exhibited more [111] facet in comparison to other shapes of AgNPs and exhibited the highest antibacterial efficacy (Roy et al., 2015). Another work done by Dong and colleagues showed that triangular-shape nanoparticles exhibited greater antibacterial property than spherical ones due to their geometric structure and geometric plane (Van Dong et al., 2012).



## **CHAPTER III**

### **MATERIAL AND METHODS**

#### **3.1 Plasmid DNA extraction and purification**

The plasmid DNA extraction and purification were prepared by alkaline lysis and phenol-chloroform extraction based on Sambrook and colleagues (Sambrook et al., 1989). A single colony of *Escherichia coli* containing the plasmid DNA, pGADT7-AD (Clontech, USA), was cultured in 4 ml Luria-Bertani (LB) broth containing 50 µg/ml of ampicillin at 37 °C for 6 h before transferring to culture in 200 ml fresh medium for another 18 h. The bacterial cells were harvested by centrifugation at 8,000 × g for 2 min. The cell pellet was re-suspended in 1 ml GTE buffer (50 mM Glucose, 25 mM Tris-HCl pH 8.0, and 10 mM EDTA pH 8.0) and lysed in 2 ml lysis buffer (0.2 N NaOH, 1% SDS) on ice for 5 min. After adding 1.5 ml neutralization buffer (5 M potassium acetate pH 5.2), the mixture was centrifuged at 12,000 × g at 4 °C for 5 min to remove cell debris. The collected supernatant was mixed with one volume of isopropanol to precipitate the DNA. After DNA pellet was collected by centrifuging, it was washed once with 70% ethanol and subsequently air-dried. The DNA was treated with RNase (300 µg/ml) at 37 °C for 1 h before purifying by adding an equal volume of phenol-chloroform solution (25:25, v/v). After a centrifugation, the aqueous phase was extracted once with chloroform. The aqueous phase was collected to precipitate the DNA by adding 2.5 volumes of ethanol and 0.1 volume of 3 M sodium acetate. The DNA pellet was collected by a centrifugation and washed once with

70% ethanol, before dissolving in sterile deionized water. The DNA concentration was determined by a Nanodrop® ND-1000 Spectrophotometer (Nanodrop Technologies, USA). The purified plasmid DNA was visualized on a 0.8% agarose gel.

### 3.2 Synthesis of AgNPs

The synthesis reaction composes of two steps, which are the seed formation and light-mediated growth. The seed formation protocol is modified from Mulfinger and colleagues (Mulfinger et al., 2007a) and the light-mediated growth is modified from Stamplecoskie and Scaiano (Stamplecoskie and Scaiano, 2010). The experiments were divided into 2 parts, the condition with strong reducing agent,  $\text{NaBH}_4$ , and weak reducing agent, glucose.

Under the condition of the strong reducing agent, 1.0 mM silver nitrate (2 ml) was added dropwise to the mixture of 2.0 mM freshly prepared  $\text{NaBH}_4$  (6 ml) and heat-denatured pGADT7 or short oligo dA and dC at room temperature with vigorous stirring. The yellow solution attributed to the reduction of  $\text{Ag}^+$  to  $\text{Ag}^0$ , indicating the formation of silver seeds wrapped around by DNA. The reaction was then exposed to LED lights to initiate a shape transformation of AgNPs. To confirm the formation of AgNPs, a spectrophotometer (Analytik Jena, Germany) was used to measure the absorbance at 300-900 nm of the reaction solution. The reactions with no light exposure and no DNA were used as the controls. To study the effects of different LED wavelengths, the reaction containing silver nitrate, heat denature DNA, and  $\text{NaBH}_4$  was exposed to blue light ( $\lambda_{\text{max}} = 460 \text{ nm}$ , 20 W), green light ( $\lambda_{\text{max}} = 520 \text{ nm}$ , 20 W), and red light ( $\lambda_{\text{max}} = 620 \text{ nm}$ , 20 W). Different shapes of AgNPs were determined from the surface plasmon resonance (SPR) peaks. To study the effect of DNA content, the

reactions containing different amounts of DNA (2, 4, and 8 pmole) were exposure to LED light for 24 h. To study the effect of reaction time, the formation of AgNPs in a time course of 24 h was studied by sampling the reactions using 4 pmole and 8 pmol DNA at 3, 6, 12, and 24 h. For the condition with oligo nucleotides, the DNA content was increased to 16 pmole and the light exposure was prolonged to 48 h.

For the condition of weak reducing agent, the reactions were performed similar to the protocol above but the 2.0 M glucose (6 ml) was added and the reaction temperature was set at 60 °C instead.

### **3.3 Characterization of the synthesized AgNPs**

#### **3.3.1 Morphology and size distribution**

The morphology and size of the synthesized AgNPs were determined by transmission electron microscope (TEM; FEI, USA). The samples were prepared by dropping the colloidal AgNPs on a carbon-coated copper holder. After air dry at room temperature, the samples were observed under TEM operating at 200 kV. The taken TEM images were analyzed by Image J software (NIH, USA) and Origin Pro 2015 software (OriginLab Corp., USA) to determine the particle size and size distribution, respectively. In addition, the selected area electron diffraction (SEAD) pattern and high resolution-transmission electron microscope (HR-TEM) were studied by a conventional transmission mode of TEM operating at 200 kV.

#### **3.3.2 The crystallographic characterization**

To study the crystalline nature of the synthesized AgNPs, X-ray diffractometer (XRD; Bruker, Germany) using Cu K $\alpha$  radiation ( $\lambda = 1.5406 \text{ \AA}$ ) was

performed. The samples were dropped on a glass slide and air-dried before transferring to XRD analysis. The XRD measurement conditions were set as following; a diffraction angle  $2\theta$  between  $30^\circ$  and  $80^\circ$ , a step-width  $\Delta 2\theta$  of  $0.02^\circ$ , and a sampling time of 10 s/step.

### **3.4 Determination of antioxidant activity of the synthesized AgNPs**

To evaluate the antioxidant activity of the synthesized AgNPs, the DPPH free radical scavenging assay was conducted according to the method of Ajayi and Afolayan (Ajayi and Afolayan, 2017). The various concentrations of the synthesized AgNPs (1.25–80.00  $\mu\text{g}/\mu\text{l}$ ) in absolute methanol (100  $\mu\text{l}$ ) were mixed thoroughly with 0.135 mM DPPH in absolute methanol (100  $\mu\text{l}$ ) followed by incubating in the dark at room temperature for 30 minutes before measuring the absorbance at 517 nm by a microplate reader (BioTek Instruments, USA). The ascorbic acid (1.25–80.00  $\mu\text{g}/\mu\text{l}$ ) was used as the standard. The scavenging abilities of the synthesized AgNPs were calculated by the following equation (Ajayi and Afolayan, 2017), where  $A_c$  is the absorbance of the DPPH control solution and  $A_s$  is the absorbance of the mixture of DPPH and sample solution.

$$\text{DPPH radical scavenging activity (\%)} = 100 \times (A_c - A_s) / A_c$$

### **3.5 Determination of antibacterial activity of the synthesized AgNPs**

Antibacterial activities of the synthesized AgNPs were determined by the minimal inhibitory concentration (MIC), the lowest concentration of AgNPs to inhibit the visible growth of the bacteria, and the minimal bactericidal concentration (MBC), the lowest concentration of AgNPs to completely kill the bacteria. In this work,

*Escherichia coli* (ATCC 25922) and *Staphylococcus aureus* (ATCC 25923) were used as the representatives of Gram-negative and Gram-positive bacteria, respectively. The antibacterial assay was followed the standard broth dilution method (Wiegand et al., 2008). Briefly, the synthesized AgNPs were two-fold serially diluted before mixing with the tested bacteria at a concentration of  $1 \times 10^6$  CFU/ml to obtain the final concentration of  $5 \times 10^5$  CFU/ml. The bacterial cultures were incubated at 37 °C with a constant shaking at 80 rpm and the optical density (OD) at 600 nm were recorded every 6 h for 24 h in order to observe the bacterial growth. The lowest concentration of AgNPs showing no visible growth of bacteria was determined as the MIC. To determine MBC, the cultures at the MIC value and two higher concentrations were spread and cultured on MH agar plates at 37 °C for 24 h. The lowest concentration of AgNPs showed no bacterial growth on the culture plates was determined as the MBC (Krishnan et al., 2015).

### 3.6 Statistical analysis

Five replicates were used for each experimental condition and at least two independent experiments were performed. The data were displayed as means  $\pm$  standard deviations. The comparison of means among groups was analyzed by one-way ANOVA and Tukey's Honestly Significant Differences with SPSS program (SPSS, USA). The *P*-value of less than 0.05 represented the different statistical significance.

## CHAPTER IV

### RESULTS AND DISCUSSION

In this work, the approaches to synthesize different shaped AgNPs were investigated by controlling several factors: reducing agents ( $\text{NaBH}_4$  and glucose), capping agents (Oligo dA, Oligo dC, and plasmid DNA), and wavelengths of LEDs (460 nm, 520 nm, and 620 nm). In addition, the synthesized AgNPs were characterized and their antioxidant and antibacterial activities were also investigated.

#### 4.1 Production of different shaped AgNPs using plasmid DNA

The synthesis of AgNPs was divided into 2 main parts, the seed formation and light induced growth. In the seed formation step,  $\text{NaBH}_4$  and glucose were used as reducing agents to reduce  $\text{Ag}^+$  to  $\text{Ag}^0$ . DNA acted as capping agent to facilitate a formation of small cluster of  $\text{Ag}^0$  into small seeds. After obtaining yellow seed solution, the different LEDs were applied to induce a formation of different shaped AgNPs.

##### 4.1.1 Plasmid DNA preparation

In this part, the long DNA strands, the 8-kb pGADT7-AD plasmid, were used to assist the formation of AgNPs. To obtain the pure plasmid DNA, the pGADT7-AD DNA were extracted from the bacterial culture and subsequently purified by alkaline lysis following by phenol-chloroform. The  $1.32 \pm 0.01$  mg of plasmid DNA were obtained per 200 ml bacterial culture and the absorbance ratio at 260 and 280 nm

of the extracted plasmid DNA was at 1.85, which was the acceptable value as a pure DNA (Boesenberg-Smith et al., 2012). Figure 4.1 shows the pattern of the extracted plasmid DNA, indicating three conformations of the plasmid DNA as seen on a 0.8% agarose gel; open circular dimer, open circular and supercoiled DNA (Dixit and Ali, 2001).

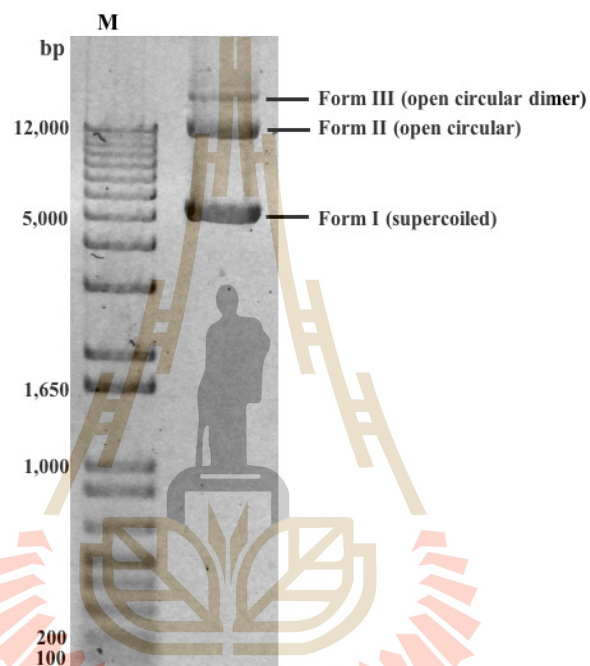


**Figure 4.1** The pattern of extracted plasmid DNA from *E. coli* containing pGADT7-AD visualized on 0.8% agarose gel.

#### 4.1.2 Effects of reducing agents and wavelength of LEDs on a formation of AgNPs

To synthesize AgNPs, the plasmid DNA (4 pmole) was heat-denatured before using in the seed formation reaction composing of  $\text{AgNO}_3$  and reducing agent ( $\text{NaBH}_4$  and glucose). To study the effect of LED wavelength on the light-induced



growth, the seed solution was irradiated to the blue (460 nm), green (520 nm), and red (620 nm) LEDs for 24 h. When glucose, considered as weak reducing agent, was used, the shape transformation of AgNP seed did not occur since the UV-Vis spectra of the seed solution after light irradiation for 1 h did not show the characteristic peak of non-spherical AgNPs but displayed the aggregated particles instead (Figure 4.2). The shape transformation by light irradiation approach require small AgNP seeds since the shape control mediated by light reported here all lead to particle growth (Stamplecoskie and Scaiano, 2010). As seen in Figure 4.2, the UV-Vis spectrum of AgNP seeds from reaction using glucose as reducing agent shows SPR peak at 450 nm indicating large size of spherical AgNPs (Agnihotri et al., 2014). Therefore, light irradiation of this large AgNP seeds possibly resulted in the aggregation.

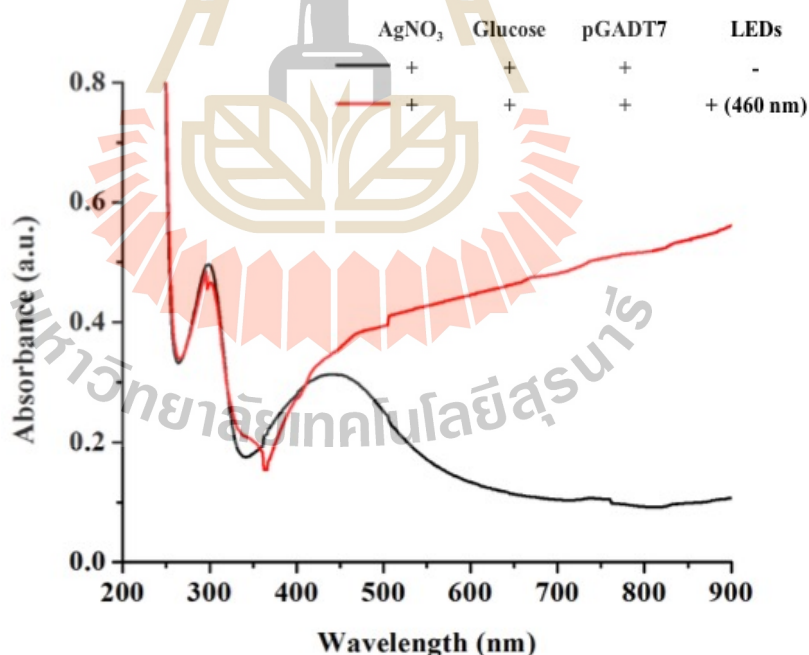


**Figure 4.2** UV-Vis spectra of the synthesized AgNPs in the reactions using glucose as weak reducing agent and pGADT7 as capping agent.

When  $\text{NaBH}_4$  was used as the reducing agent, the reactions exposed to green and red LEDs appeared as yellow color with the surface plasmon resonance (SPR) peaks at 406 and 404 nm, respectively (Figure 4.3). Based on the reaction color and the characteristic SPR peaks, it was likely that the formed AgNPs were nanospheres (Agnihotri et al., 2014). In contrast, the reaction exposing to the blue LED appeared in green color with the presence of two SPR peaks at 412 and 595 nm, suggesting the formation of non-spherical AgNPs (Tao et al., 2008). Although the right-shifted SPR peak may indicate the formation of larger sizes of AgNPs (Agnihotri et al., 2014), the newly emerged SPR peak in the range of 495 – 630 nm aside from the original SPR peak of small silver seeds at 416 – 418 nm is the characteristics of non-spherical AgNPs (Liu et al., 2010). The control reactions with no light exposure and no DNA remained in yellow color with the SPR peaks at 420 and 413 nm, respectively, indicating the presence of spherical AgNPs (Agnihotri et al., 2014). The synthesized AgNPs in the reaction without a capping agent could be stable for few weeks since the absorbed borohydride ions on the particle surface provided the repulsive electrostatic forces to prevent the particle aggregation (Mulfinger et al., 2007b). Taken all results together, the optimal LED light and DNA were considered as the key factors for transforming the spherical seeds of AgNPs to the other shapes.

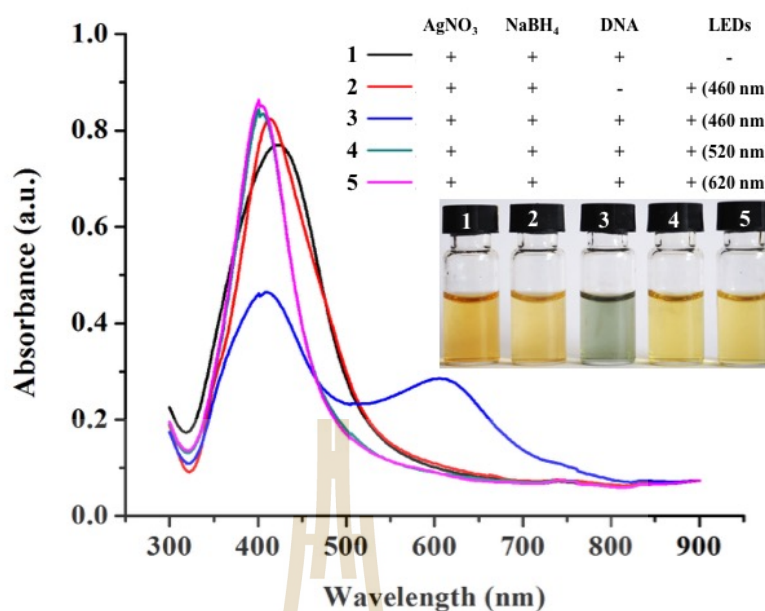


**Figure 4.3** UV–Vis spectra of the formed AgNPs under different conditions.

#### 4.1.3 Effects of DNA content on a formation of AgNPs

The concentration of the capping agent is another factor that affected the shape conversion of AgNPs (Tang et al., 2015), therefore, the reactions containing different DNA amounts (2–8 pmole) under a blue LED irradiation for 24 h were monitored. As seen in Figure 4.4, the reaction containing 2 pmole DNA could not induce a shape-conversion of AgNPs as indicated by the remained yellow color and the characteristic SPR peak at 413 nm (Agnihotri et al., 2014). Upon the increase of DNA amount to 4 pmole, the shape-transformation of non-spherical AgNPs was successfully occurred as determined by the changed color to green and the characteristic SPR peaks at 412 and 595 nm, which corresponded to the in-plane dipole plasmon resonance of possibly formed hexagonal and triangle AgNPs (Liu et al., 2010). Similarly, the reaction containing 40  $\mu$ g DNA could induce a formation of non-

spherical AgNPs but the reaction turned to orange color and its SPR peaks were at 424 and 562 nm, which was likely attributed to the formed hexagonal AgNPs (Liu et al., 2010).

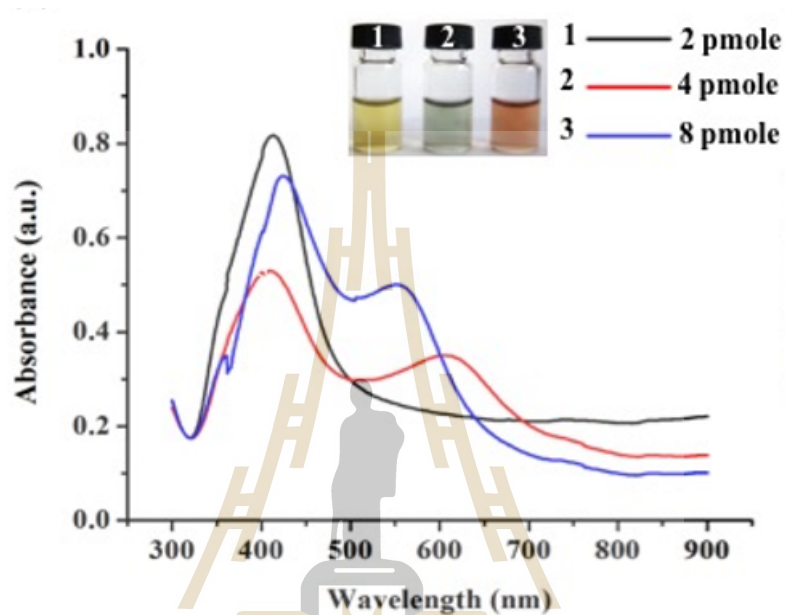


**Figure 4.4** UV-Vis spectra of the synthesized AgNPs in the reactions containing different amount of pGADT7-AD at 24 h under the blue LED irradiation.

#### 4.1.4 Effects of the synthesis time on a formation of AgNPs

The UV-Vis spectra of the formed AgNPs in the reactions containing 4 and 8 pmole of pGADT7-AD plasmid DNA under blue light irradiation were also monitored in a time course of 24 h. In the reactions using 4 pmole DNA, the formation of non-spherical AgNPs was first detected at 6 h as determined by the changes from yellow to orange and green colors and the SPR characteristic peaks at 412 and 595 nm (Figure 4.5(A)). When the irradiation times were increased, the SPR peaks were

slightly right-shifted to the longer wavelengths. Similarly, in the reactions using 8 pmole DNA the formation of non-spherical AgNPs was first detected at 6 h but the reaction color turned to orange, while the SPR peaks were observed at 424 and 562 nm (Figure 4.5(B)). These results confirmed the effect of DNA content on the induction of non-spherical AgNPs upon a blue light exposure. The synthesized AgNPs from the condition containing 4 pmole DNA under 24-h blue light irradiation was chosen to compare with the rests of the conditions in the next parts.

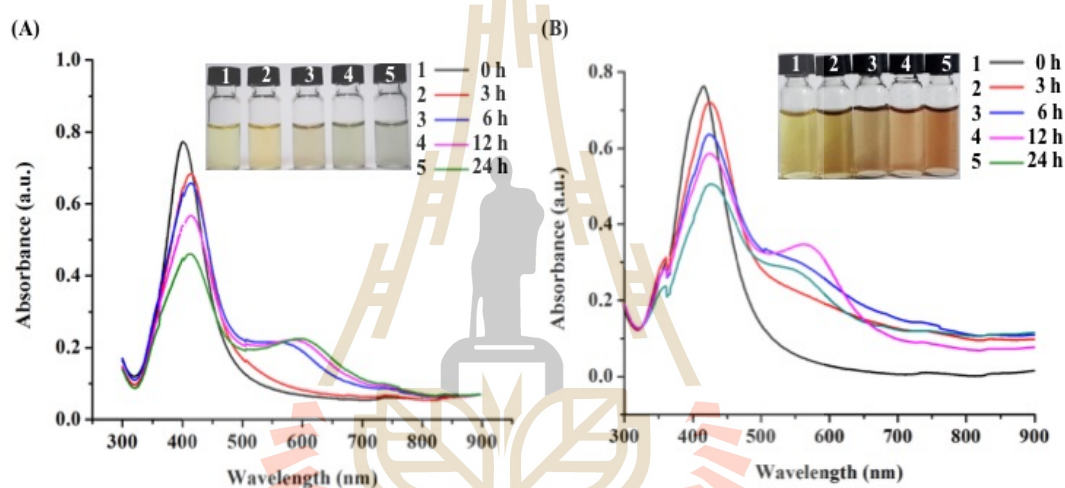


**Figure 4.5** UV-Vis spectra of the synthesized AgNPs in the reactions containing (A) 4 pmole and (B) 8 pmole of pGADT7-AD in a time course of 24 h under the blue light irradiation.

#### 4.1.5 Characterization of the plasmid-capped AgNPs

The representative TEM images of the plasmid-capped AgNPs are shown in Figure 4.6. For the reaction using 2 pmole DNA (Figure 4.6(A)), the formed AgNPs were all spherical with the average diameter of  $11.66 \pm 4.11$  nm. The TEM image of the reaction using 4 pmole DNA revealed the AgNPs in hexagonal (26%) and corner-

truncated triangle (8%) shapes in addition to spherical (66%) shape (Figure 4.6(B)), which were correlated to the characteristic SPR peaks of AgNPs at 412 and 595 nm (Liu et al., 2010). Under this condition, the average sizes of spherical, hexagonal, and corner-truncated triangle AgNPs were  $12.32 \pm 2.22$ ,  $23.03 \pm 6.62$ , and  $15.84 \pm 4.31$  nm, respectively. In the reaction using 8 pmole DNA, only two particle shapes were detected (Figure 4.6(C)); spherical (80%) and hexagonal (20%), which were also correlated to the characteristic SPR peaks of AgNPs at 424 and 562 nm (Liu et al., 2010). The average sizes of spherical and hexagonal AgNPs under this condition were  $12.09 \pm 3.24$  and  $16.28 \pm 3.63$  nm, respectively. This result suggested that the ratio of  $\text{Ag}^+$  and DNA affected the formation of non-spherical AgNPs. In this work, the percentage of non-spherical AgNPs was not high, the adjustment of some factors might increase the production of non-spherical AgNPs, such as pH (Yu et al., 2011) and photon flux (Lee et al., 2013), which the further investigation is needed. We hypothesize that the possible mechanism of the light-induced shape transformation is consisted of two steps; the small seed formation and the light-induced growth of non-spherical shape. The  $\text{Ag}^+$  ions are reduced to  $\text{Ag}^0$  rapidly by the strong reducing agent, which were wrapped around by the ssDNA strands to form the small clusters of silver seeds (Chumpol and Siri, 2017). Their growth into the anisotropic shape is assisted by the LED-light activation and the selective binding of nitrogenous bases on particular planes of nanoparticles (Li et al., 2016). The electromagnetic (EM) field produced by LED-light can excite and cause the coalescence of the nanoparticle seeds (Stamplecoskie and Scaiano, 2010), which the pattern of coalescence may be related to the bindings between DNA and AgNPs. Due to the negatively charged functional groups of DNA chain, it is likely that DNA may preferentially bind to the [111] planes

of planar seeds, thus covering the top and bottom surfaces (Yi et al., 2013). As the result, the addition of Ag atom on this plane is blocked; therefore, the silver atoms preferentially deposit on the [100] plan leading to the growth of triangular and hexagonal plates (Li et al., 2016). In this work, the blue LED is only light source that provide enough energy to drive the coalescence of small seeds due to its high energy, which in accordance with previous report (Stamplecoskie and Scaiano, 2010). In contrast, the green and red LEDs that have longer wavelength resulting in lower energy could not provide enough energy to drive the shape transformation of AgNPs as analyzed by TEM images (data not shown).

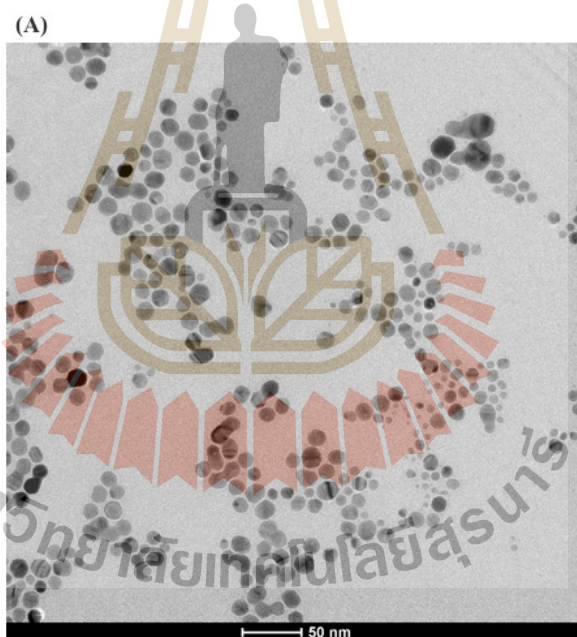


**Figure 4.6** Representative TEM images of the plasmid-capped AgNPs in the reactions containing (A) 2 pmole, (B) 4 pmole, and (C) 8 pmole of DNA.

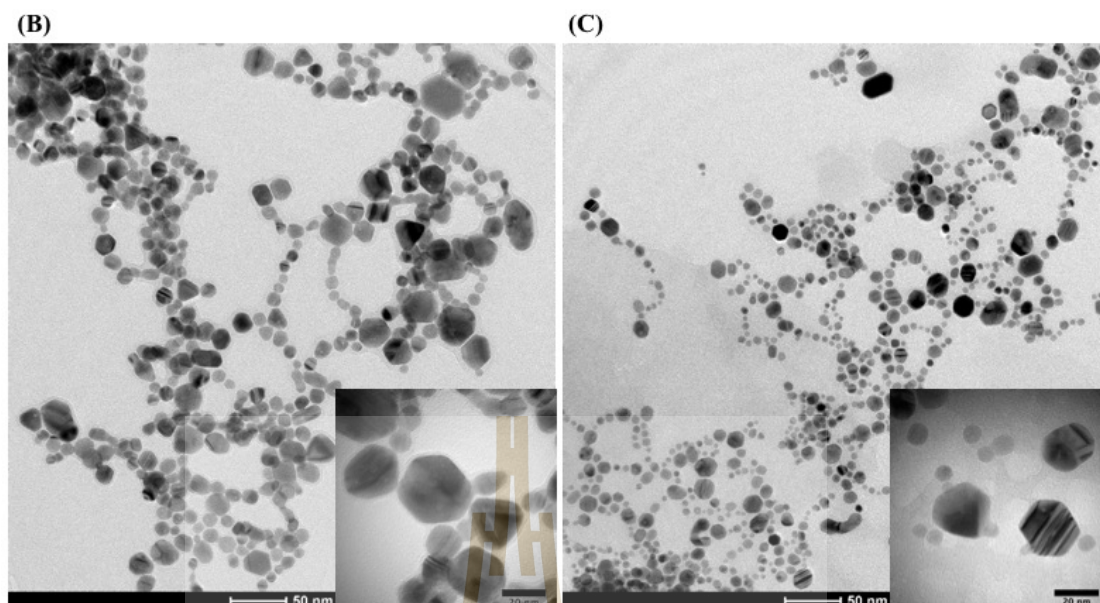


**Figure 4.6** Representative TEM images of the plasmid-capped AgNPs in the reactions containing (A) 2 pmole, (B) 4 pmole, and (C) 8 pmole of DNA (Continued).

The identity of synthesized AgNPs of the reactions using 4 pmole of pGADT7, was further analyzed by XRD, SEAD-TEM, and HR-TEM. The XRD analysis was conducted to confirm the crystalline nature of the synthesized AgNPs. Figure 4.7(A) shows the XRD pattern of pGADT7 AD capped AgNPs, which two major peaks at  $38.4^\circ$  and  $44.7^\circ$ , corresponding to the [111] and [200] facets, respectively were detected. In general, the high population of hexagonal and corner-truncated triangle AgNPs exhibits the intense [111] peak due to their [111]-covering faces (Park et al., 2016). The presence of the peak corresponding to the [200] facet in this result possibly attributed to the population of spherical AgNPs in the reactions. The SEAD-TEM patterns demonstrated four diffraction rings, which were indexed as [111], [200], [220], and [311] planes (Figure 4.7(B)), well corresponding to the Bragg's planes of face-centered cubic (fcc) structure of silver (Szeremeta et al., 2014).



These concentric rings revealed that the synthesized AgNPs were polycrystalline in nature. The HR-TEM image of the synthesized AgNPs as seen in Figure 4.7(C) revealed their d-spacing value of 0.23 nm, in a good agreement with the lattice fringe [111] plane of fcc structure of silver (Al-Ghamdi and Mahmoud, 2014).

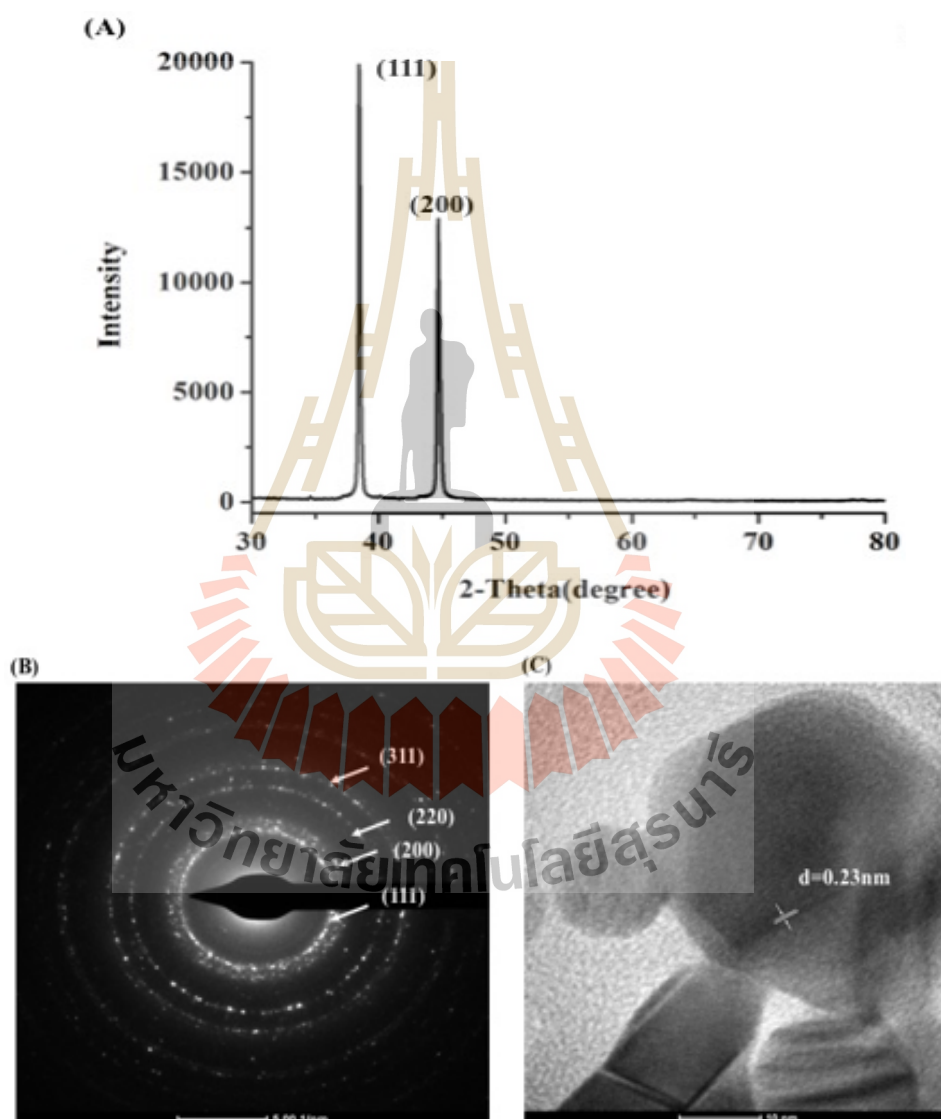


**Figure 4.7** Characterization of the plasmid-capped AgNPs (4 pmole). (A) XRD pattern, (B) SAED-TEM, and (C) HR-TEM.

#### 4.1.6 Antibacterial activity of the plasmid-capped AgNPs

The broad-spectrum antibacterial activity is one of the interesting properties of AgNPs, which this property is depended on their size and shape (Hong et al., 2016). To investigate the antibacterial activity of the synthesized AgNPs, a micro-broth dilution method was performed. The growths of the representative Gram-negative (*E. coli*) and Gram-positive (*S. aureus*) bacteria in response to various concentrations of synthesized AgNPs in a time course of 24 h were monitored. The results showed that all synthesized AgNPs exhibited the antibacterial activity against both bacterial strains in a dose-dependent response. Figure 4.8 shows the growths of *E. coli* and *S. aureus* in response to the plasmid-capped AgNPs (the reaction using 4 pmole plasmid DNA) in a range of 5-80  $\mu\text{g/ml}$ . The minimum inhibition concentration (MIC) values of the produced AgNPs against *E. coli* and *S. aureus* were equally at 40  $\mu\text{g/ml}$ . The minimum bactericidal concentration (MBC) values of the AgNPs against *E. coli* was 40  $\mu\text{g/ml}$ , while the MBC values against *S. aureus* were higher at 80  $\mu\text{g/ml}$ . The *S. aureus* was less susceptible to AgNPs due to the thicker peptidoglycan layer of its cell wall (Janthima et al., 2017).

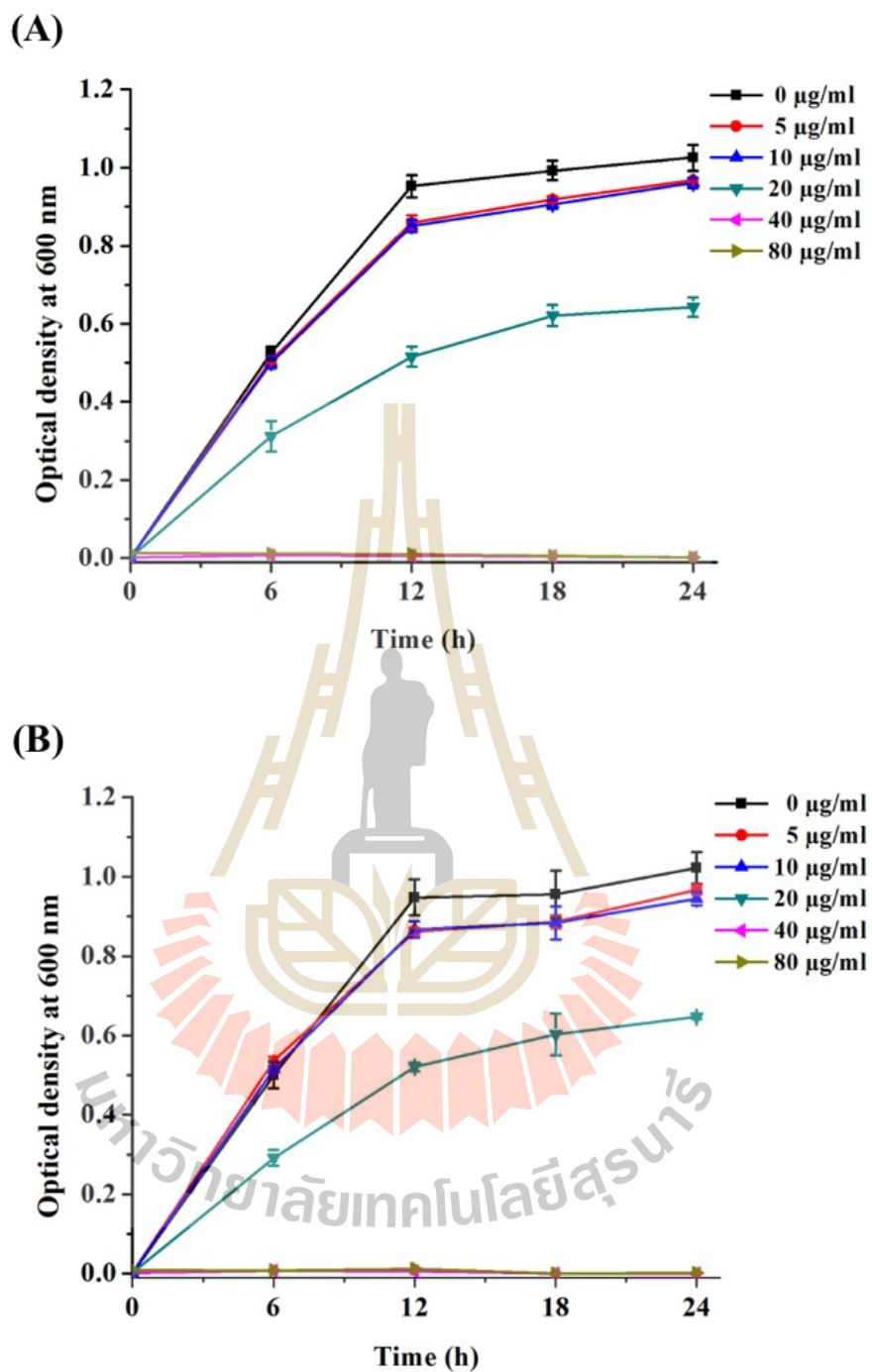


**Figure 4.8** Growth curves of (A) *E. coli* and (B) *S. aureus* in response to different concentrations of the synthesized AgNPs in a time course of 24 h.

#### 4.1.7 Antioxidant activity of the plasmid-capped AgNPs

The antioxidant activity of the plasmid-capped AgNPs was also evaluated by the DPPH scavenging assay based on the activity of the tested samples to reduce DPPH radicals, which is expressed as % DPPH inhibition (Patra et al., 2016). The maximum absorption of the DPPH radicals at 517 nm is decreased upon the reduction by the tested samples together with the decolorization of the DPPH solution from violet color (the free radical form, diphenyl picrylhydrazyl) to yellow color (the non-free radical form, diphenyl picrylhydrazine). The DPPH radical scavenging activities of the positive control, ascorbic acid, and the plasmid-capped AgNPs at 5–40 µg/ml are shown in Figure 4.9. With increasing in concentrations, the plasmid-capped AgNPs exhibited the antioxidant activity in the dose-dependent response. The inhibition concentration 50% (IC<sub>50</sub>) values of the plasmid-capped AgNPs was  $7.34 \pm 0.76$  µg/ml, which was lower than that of the control ascorbic acid ( $4.41 \pm 0.13$  µg/ml). Nevertheless, the antioxidant activity of synthesized AgNPs was greater than many reported activities of AgNPs, which were in a range of 70–400 µg/ml (Huo et al., 2017; Kharat and Mendhulkar, 2016; Moteriya and Chanda, 2016). In contrast, some synthesized AgNPs were reported to exhibit the greater antioxidant activity than the AgNPs in this work, especially ones synthesized using plant extracts as capping agents, which the strong antioxidant activity of these synthesized AgNPs partially attribute to the antioxidant activity of the capping agents (Khan et al., 2016). Since the plasmid DNA, the capping agent in this work, exhibited less or no antioxidant activity, the synthesized AgNPs in this work exhibited the antioxidant activity not as high as some reported AgNPs using capping agents possessing antioxidant activity.

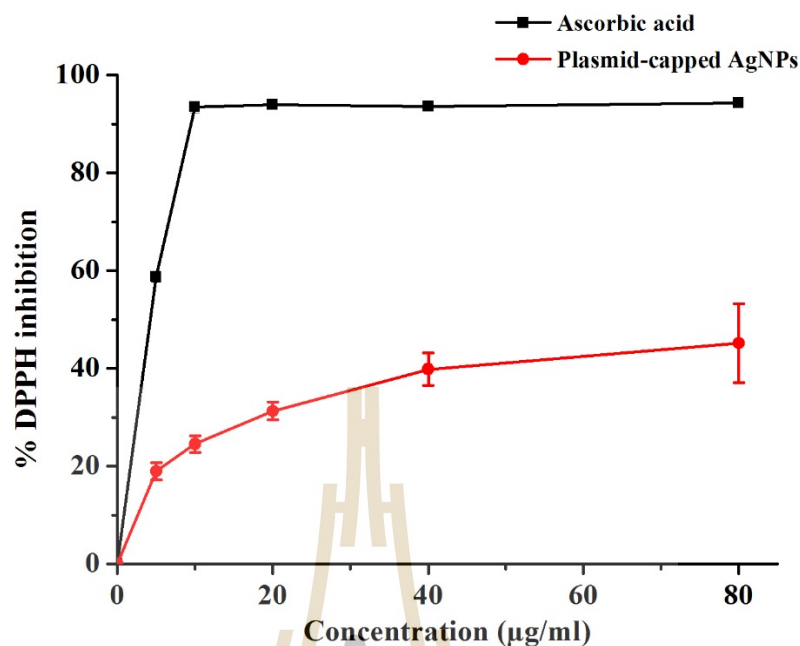


**Figure 4.9** DPPH free radical scavenging activity of the plasmid capped AgNPs and positive control, ascorbic acid.

## 4.2 Production of different shaped AgNPs using oligo dA and dC

The oligo dA<sub>30</sub> (A30) and dC<sub>30</sub> (C30), the short single stranded DNA with 30 bases of adenine and cytosine, respectively, were used as capping agents to study the effect of DNA sequence on the light-induced shape transformation of AgNPs.

### 4.2.1 Effect of DNA content and synthesis time on a formation of AgNPs using A30

To investigate the effect of DNA content on the photo-induced shape conversion, the different DNA amounts (4, 8, and 16 pmole) were added into seed formation reaction followed by a blue LED irradiation for 48 h. In case of A30, Figure 4.10 demonstrates that in the reaction containing 4 pmole, there was the presence of the SPR peak at 404 nm, suggesting a formation of spherical AgNPs. However, when

the DNA contents were increased to 8 and 16 pmole, in addition to the main SPR peak at 404 nm, the new SPR peak at 448 nm was observed. When the DNA amount was increased to 16 pmole, the SPR peak at 404 nm, corresponded to spherical seeds, was decreased visibly while the shoulder peak at 448 nm became more clear.

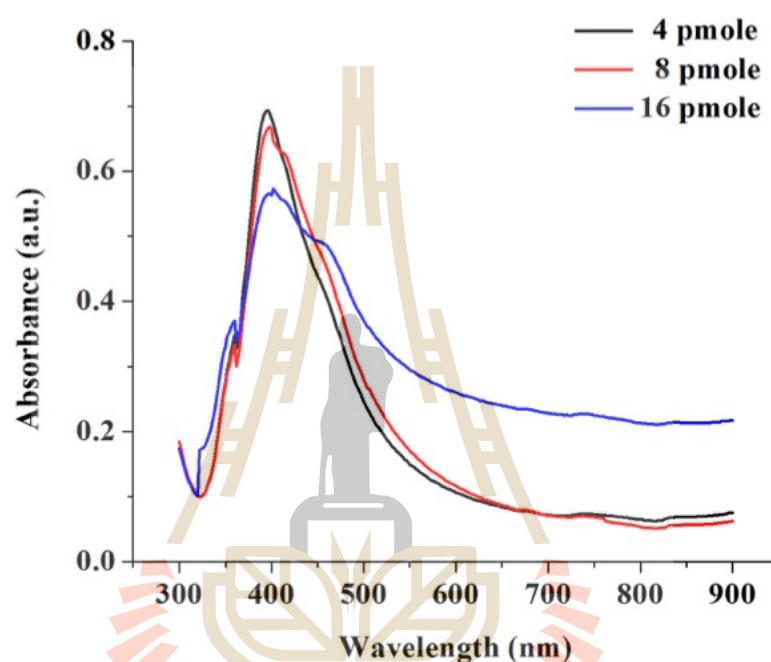


**Figure 4.10** UV-Vis spectra of the synthesized AgNPs in the reactions containing different amounts of A30 under the blue light irradiation for 48 h.

The reaction containing 16 pmole of A30 under blue light exposure was further analyzed by observing the reaction at 24 and 48 h. The UV-Vis spectra in Figure 4.11 revealed that the second small peak at 448 nm firstly appeared at 24 h of exposure. With increased times, the SPR peak intensity at 404 nm, which attributed to spherical silver seeds, was decreased as the time increased. These characteristic SPR peaks and the change of color from light yellow to deeper shade possibly

indicated that the spherical AgNPs were increased in size as light exposure was prolonged (Stamplecoskie and Scaiano, 2010).

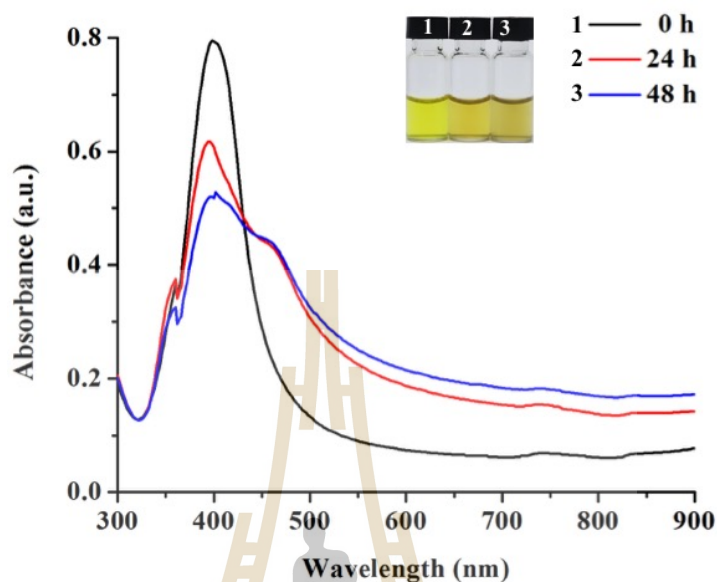


**Figure 4.11** UV-Vis spectra of the synthesized AgNPs in the reactions containing 16 pmole of A30 under the blue light irradiation in a time course of 48 h.

#### 4.2.2 Effect of DNA content and synthesis time on a formation of AgNPs using C30

To determine the effect of different C30 contents on the formation of AgNPs, the reactions containing 4, 8, and 16 pmole C30 were performed under the blue light irradiation for 48 h, which the results are shown in Figure 4.12. With increased C30 contents, two SPR peaks were observed at 400 and 454 nm, suggesting the formation of both spherical and non-spherical AgNPs. The characteristic SPR peak at 400 nm was likely the spherical AgNPs, while the characteristic peak at 454 nm suggested the formation of non-spherical AgNPs. With increased C30 contents, the SPR peak attributed to spherical AgNPs was decreased and slightly shifted to 404 nm,

while the absorbance value of the new peak at 454 nm was elevated. The changed color to green and the presence of two SPR peaks indicated the success of light-mediated shape transformation of AgNPs by using C30 as capping agent.

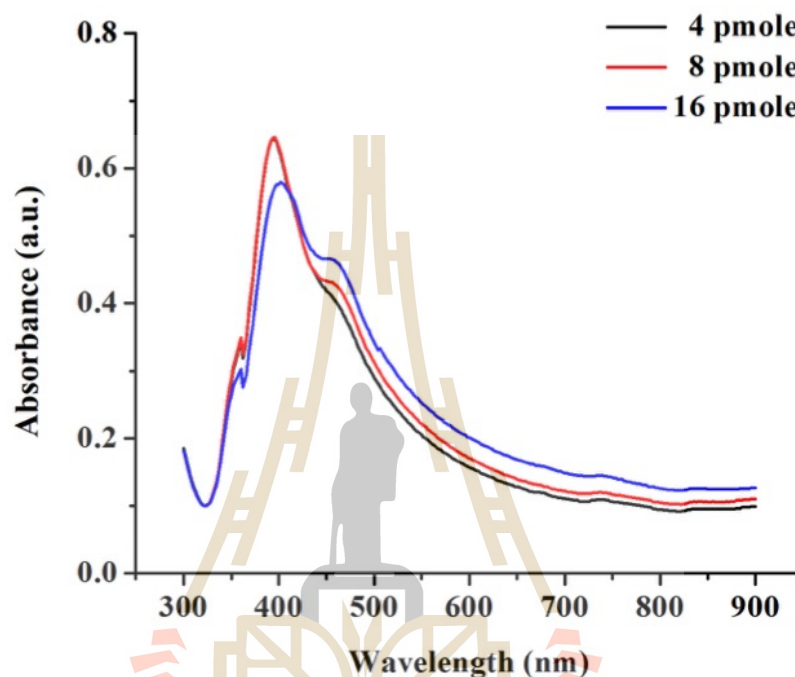


**Figure 4.12** UV–Vis spectra of the synthesized AgNPs in the reactions containing different amounts of C30 under the blue light irradiation for 48 h.

The effect of irradiation times on the formation of AgNPs is shown in Figure 4.13. The conversion of small spherical seeds to non-spherical AgNPs was first detected at 24 h as determined by the changes from yellow to green colors and the emerged SPR characteristic peaks at 454 nm. At the end of irradiation, the color turned to more greenish shade with an increase in absorbance at 454 nm apart from the SPR peak at 408 nm corresponding to the characteristics of non-spherical AgNPs (Stamplecoskie and Scaiano, 2010).



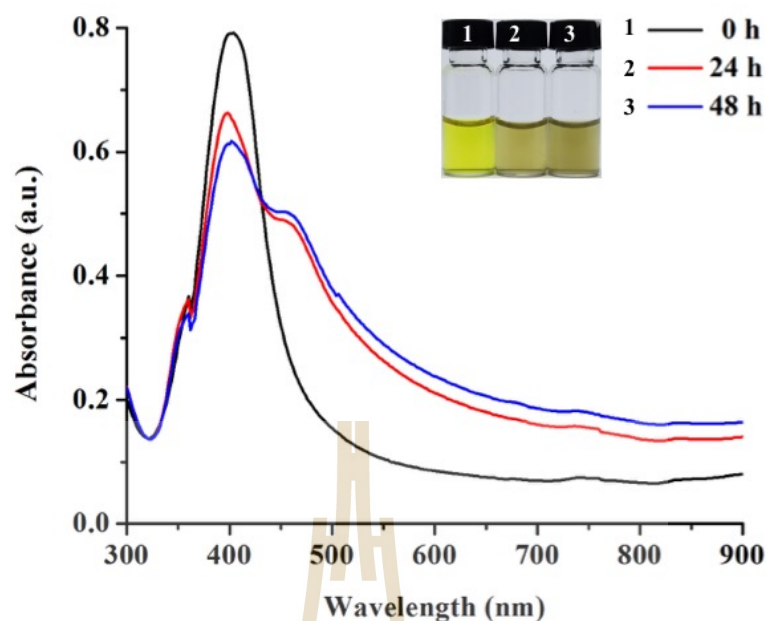


**Figure 4.13.** UV–Vis spectra of the synthesized AgNPs in the reactions containing 16 pmole of C30 under the blue light irradiation in a time course of 48 h.

#### 4.2.3 Characterization of the A30-capped and C30-capped AgNPs

The TEM micrograph revealed that A30-capped AgNPs with DNA content of 16 pmole led to the formation of spherical AgNPs (Figure 4.14(A)) with a diameter of  $26.53 \pm 6.96$  nm. The size distribution of A30-capped AgNPs from this reaction ranged from 15.35 to 49.47 nm (100 particles). Even though the second peak is the character of non-spherical AgNPs, the second peak at 448 nm of A30-capped AgNPs possibly resulted from the population of large sized AgNPs in spherical shape since this SPR peak and deep yellow color of the product corresponded with the AgNP size in the range of 30-50 nm (Agnihotri et al., 2014). In this case, we hypothesize that A30 equally bind to both planes of Ag seeds leading to the same rate of Ag atom deposit in the light-induced growth step. As a result, the spherical AgNPs were obtained from this reaction.

The TEM image of C30-capped AgNPs (Figure 4.15(A)) shows a variety of nanoparticles: spherical, truncated hexagonal, flat elongated (rod-like), and truncated triangular shapes with the average diameter of  $24.38 \pm 6.02$  nm. The truncated hexagonal and triangular morphologies resulted from the selective growth on [100] direction as mentioned in the plasmid-capped AgNPs. The flat elongated AgNPs founded in this reaction possibly resulted from the growth of flat rounded AgNPs (Cardoso-Avila et al., 2015), which the etching of the protruding edges of hexagonal AgNPs led to this flat rounded shape (Cathcart et al., 2009). In case of using A30 and C30 as the capping agent, the results contradicted to the hypothesis regarding to the possible binding sites on silver seeds. According to the possible sites of adenine and cytosine for bonding with AgNPs in Figure 2.2, A30 and C30 were proposed to have the plausible binding sites similar to citrate and PVP, which preferentially bind to the [111] and [100] planes of silver seeds, respectively. However, the results revealed that A30 equally bound to both planes of Ag seeds, while C30 selectively bound to the [100] plane, leading to the large spherical and a variety of nanoplate structure, respectively. In nature, single strand nucleotides including ssDNA and RNA are in spiral shape (Liang et al., 2006); they are not in linear form as depicted in Figure 2.2. Therefore, the possible site of each short oligonucleotide for binding to AgNPs may be different from the hypothesis.

The characterization of the A30-capped and C30-capped AgNPs was studied using XRD and SAED-TEM analyses. The results are shown in Figure 4.14 and 4.15. The XRD pattern of A30-capped AgNPs (Figure 4.14(B)) and C30-capped AgNPs (Figure 4.15(B)) demonstrated four diffraction peaks in the  $2\theta$  range of  $30^\circ$ - $80^\circ$ , which were indexed as [111], [200], [220], and [311] planes of the Bragg's planes

of face-centred cubic (fcc) structure of silver, in agreement with the standard data (Joint committee on powder diffraction standards (JCPDS) file no. 89-3722 (Anandalakshmi et al., 2016). In addition, the diffraction peak in the  $2\theta$  of  $32.3^\circ$  was found in the XRD pattern of A30-capped and C30-capped AgNPs, which matched with [111] plane of fcc structure of  $\text{Ag}_2\text{O}$  according to JCPDS No. 76-1393 (Zhu et al., 2012). In this case, it was likely that some formed AgNPs were oxidized to  $\text{Ag}_2\text{O}$  (Levard et al., 2012) during synthesized reaction or sample preparation for characterization.

The SAED-TEM patterns of the A30-capped and C30-capped AgNPs are shown in Figure 4.14(C) and 4.15(C) revealing the polycrystalline structure of the synthesized AgNPs. The four-diffraction rings in [111], [200], [220], and [311] planes were indexed to the face-centered cubic (fcc) crystal structure of Ag (Szeremeta et al., 2014). Similar to XRD result, the innermost diffraction ring of the A30-capped and C30-capped AgNPs corresponded to the [111] plane of fcc structure of  $\text{Ag}_2\text{O}$  aside from four characteristic diffraction rings of Ag (Pardha-Saradhi et al., 2014).

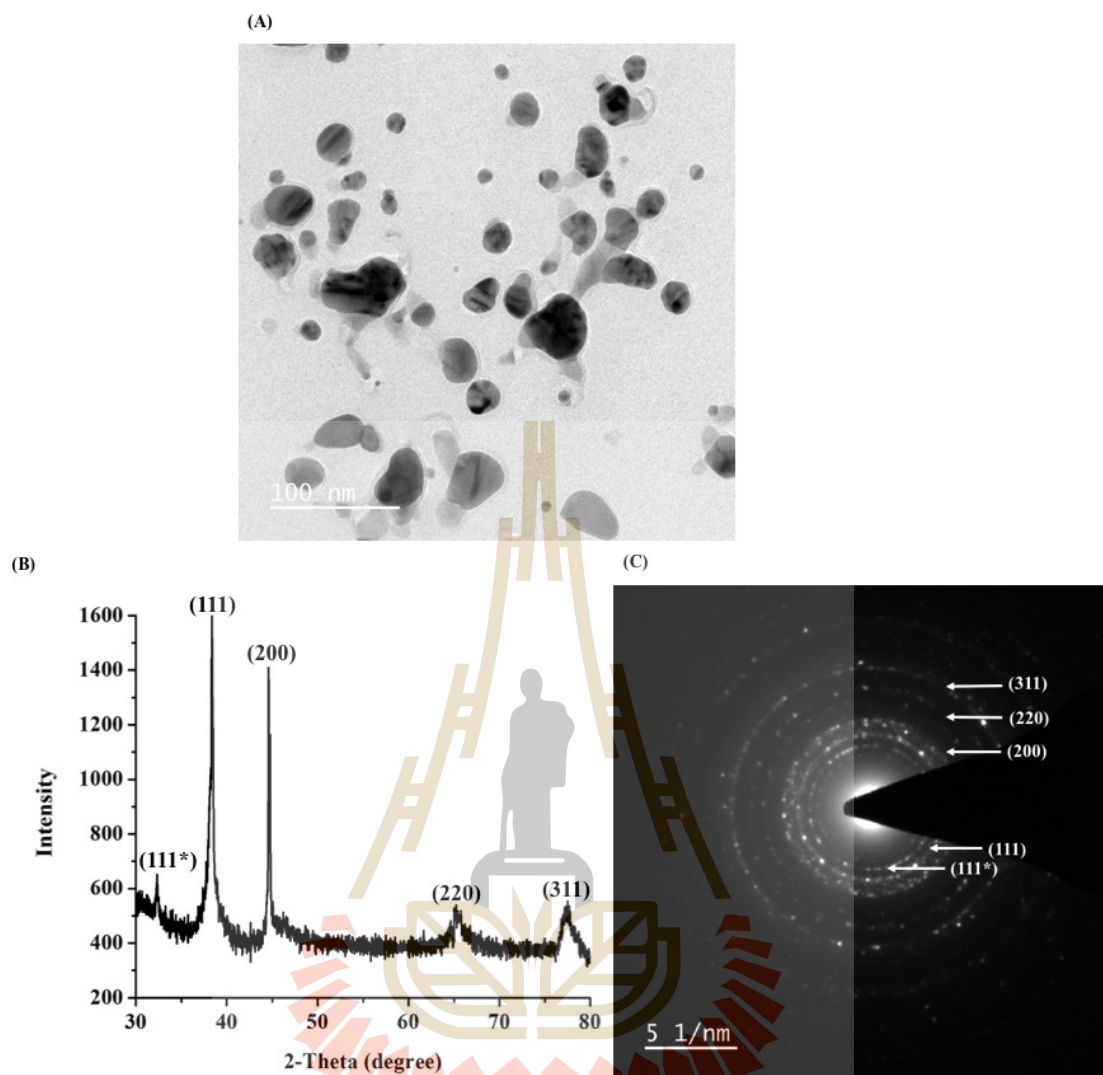


**Figure 4.14** Characterization of the A30-capped AgNPs as analyzed by (A) TEM, (B) XRD, and (C) SAED-TEM.

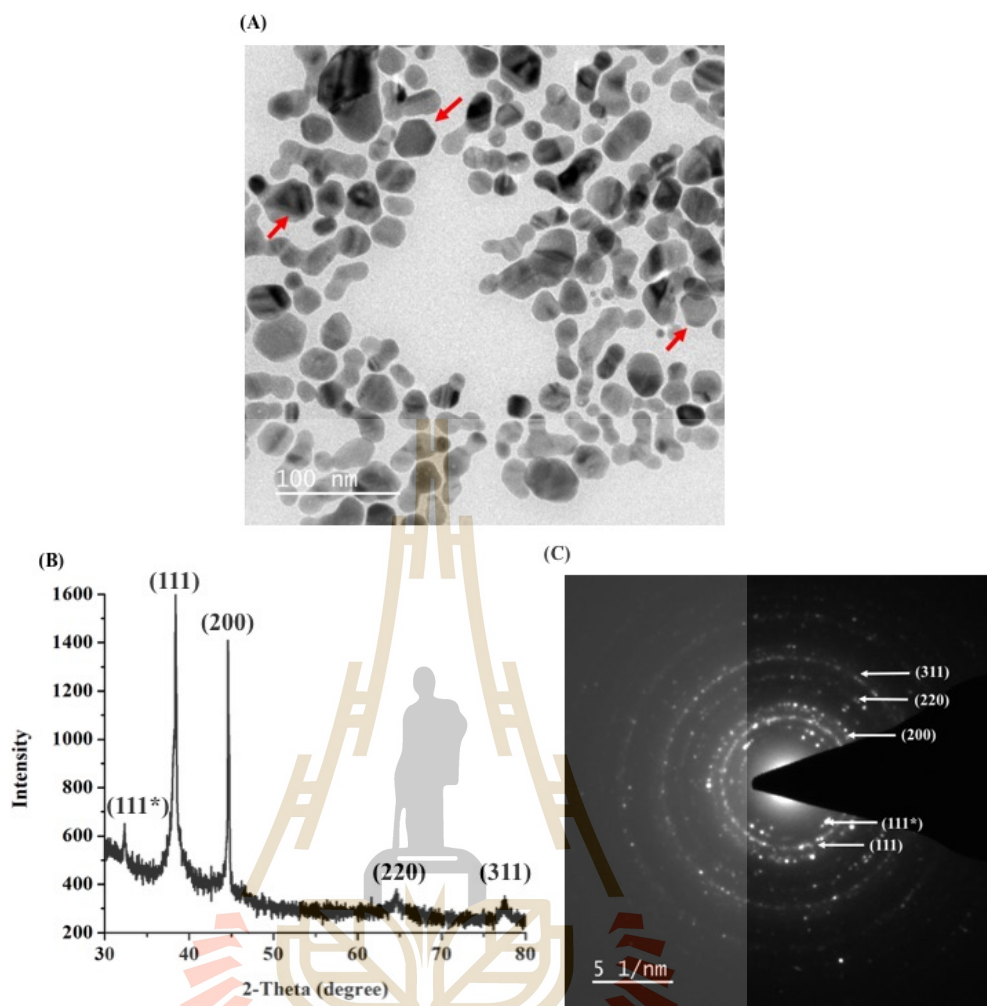


**Figure 4.15** Characterization of the C30-capped AgNPs as analyzed by (A) TEM, (B) XRD, and (C) SAED-TEM.

#### 4.2.4 Antibacterial activity of the synthesized AgNPs

The bacterial inhibition activities of A30-capped and C30-capped AgNPs against *E. coli* and *S. aureus* are shown in Figures 4.16 and 4.17, in which dose-dependent activities are revealed. From the growth curves, the MIC values of A30-capped and C30-capped AgNPs against both bacteria were determined, which were equally at 160  $\mu\text{g/ml}$ . In addition, the MBC values of the A30-capped and C30-capped AgNPs were determined, which their MBC values against *E. coli* were equally at 160  $\mu\text{g/ml}$ , while their MBC values against *S. aureus* were also equally at 320  $\mu\text{g/ml}$ .

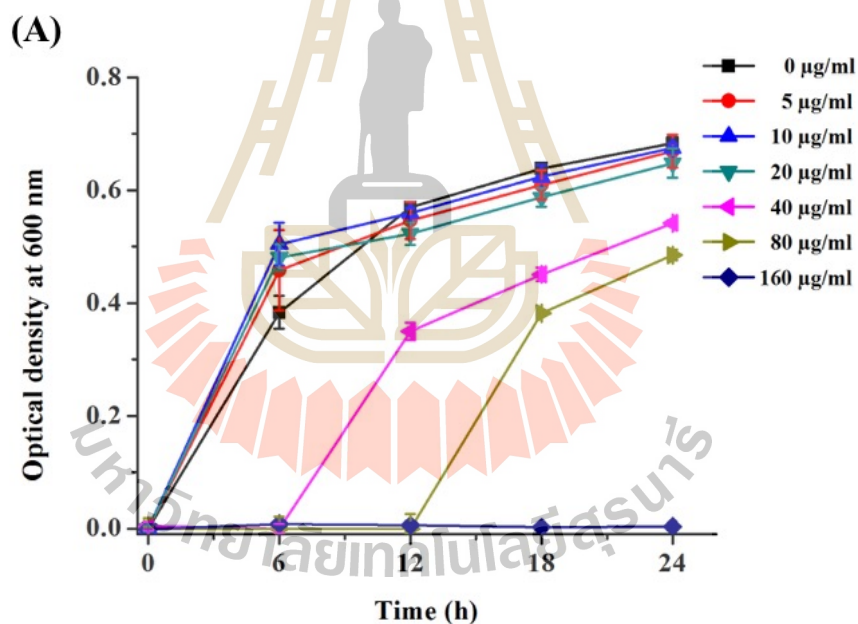


**Figure 4.16** Growth curves of (A) *E. coli* and (B) *S. aureus* in response to different concentrations of the A30-capped AgNPs in a time course of 24 h.

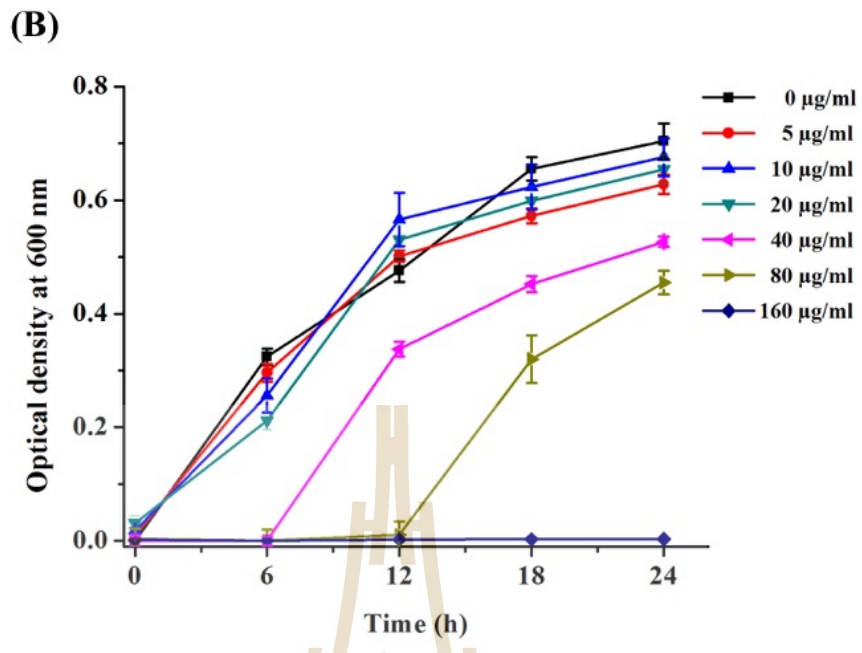


**Figure 4.16** Growth curves of (A) *E. coli* and (B) *S. aureus* in response to different concentrations of the A30-capped AgNPs in a time course of 24 h (Continued).

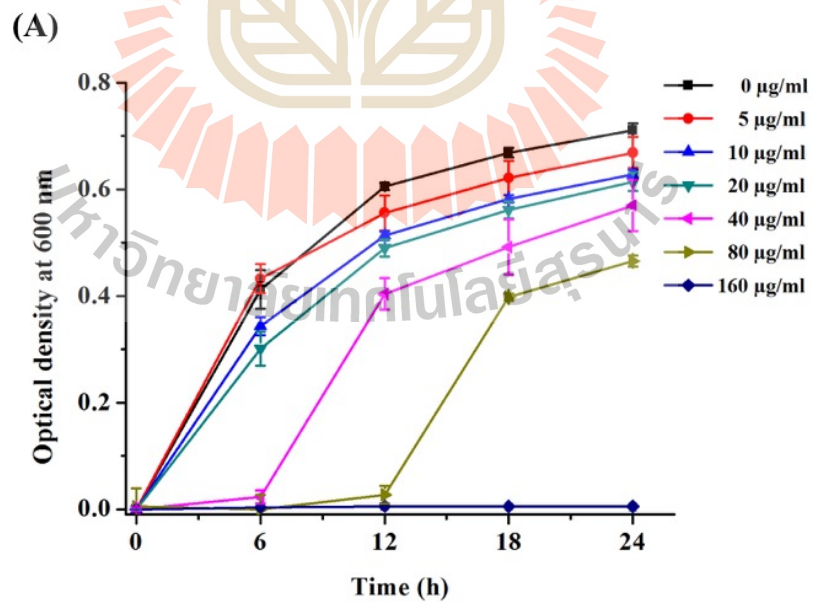


**Figure 4.17** Growth curves of (A) *E. coli* and (B) *S. aureus* in response to different concentrations of the C30-capped AgNPs in a time course of 24 h.

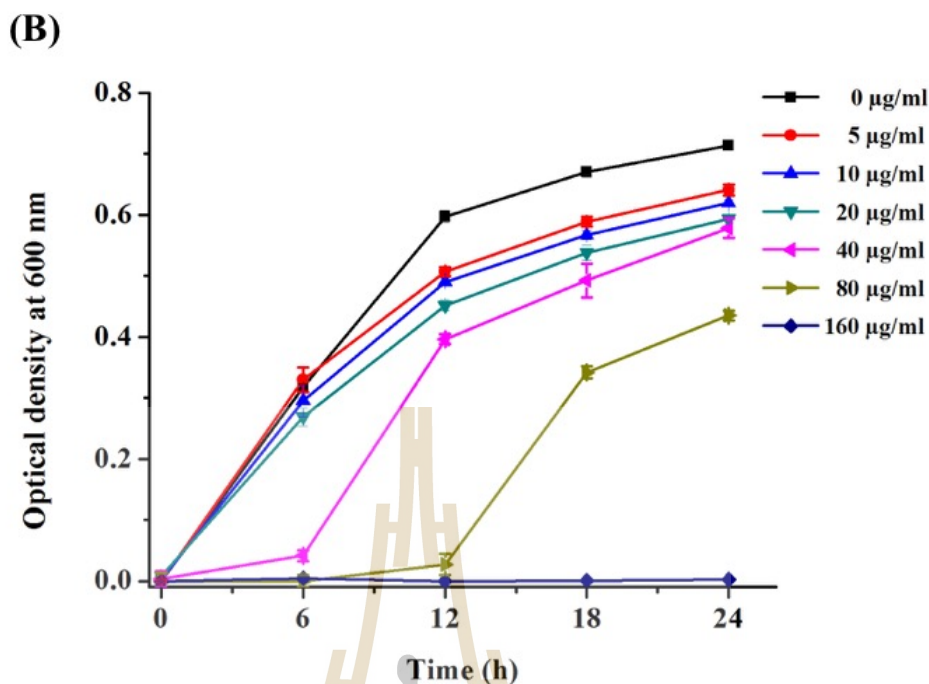


**Figure 4.17** Growth curves of (A) *E. coli* and (B) *S. aureus* in response to different concentrations of the C30-capped AgNPs in a time course of 24 h (Continued).

#### 4.2.5 Antioxidant activity of the synthesized AgNPs

Similar to the plasmid-capped AgNPs, the A30-capped and C30-capped AgNPs exhibited the antioxidant activities in the dose-dependent responses (Figure 4.18). The IC<sub>50</sub> values of A30-capped and C30-capped AgNPs were at  $6.78 \pm 0.83$  and  $6.98 \pm 0.46$  µg/ml, respectively. Even though the IC<sub>50</sub> values of the synthesized AgNPs were lower than that of the control ascorbic acid ( $4.41 \pm 0.13$  µg/ml), their antioxidant activities were higher than a number of reported activities of AgNPs as mentioned before.



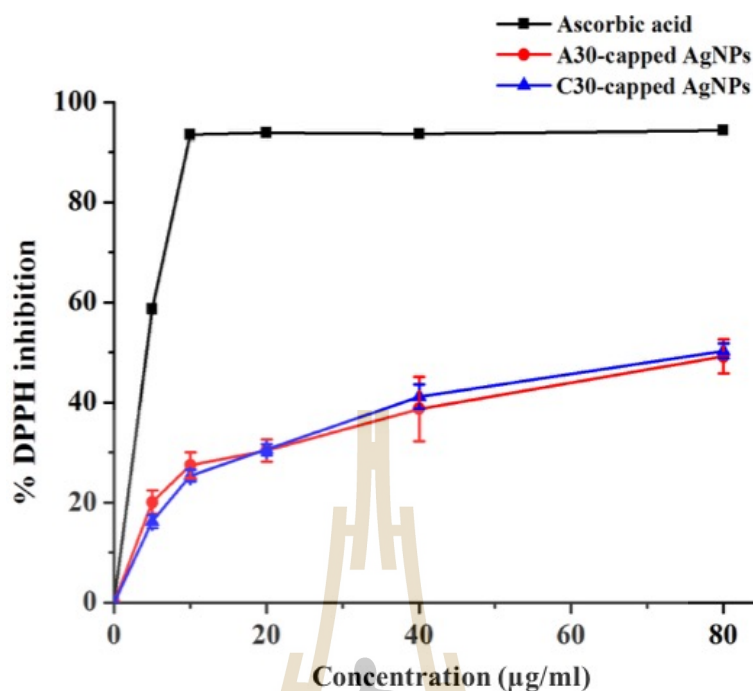


**Figure 4.18** DPPH free radical scavenging activity of the A30-capped AgNPs, C30-capped AgNPs, and ascorbic acid (positive control).

### 4.3 Comparison of the plasmid-capped, A30-capped, and C30-capped AgNPs

#### 4.3.1 Morphology, average sizes, and characterization

The comparison of the formation of plasmid-capped, A30-capped, and C30-capped AgNPs is summarized in Table 4.1. For the reaction using plasmid DNA, the condition using 4 pmole plasmid DNA and blue LED exposure for 24 h could give rise to non-spherical AgNPs aside from the spherical ( $12.32 \pm 2.22$ ) AgNPs; hexagonal ( $23.03 \pm 6.62$  nm) and corner-truncated triangle ( $15.84 \pm 4.31$  nm). For the reaction using C30 DNA, the mixture of non-spherical and spherical AgNPs was also obtained, however, the reaction required four times higher DNA content and two times longer

exposure time. Under this condition, spherical, truncated hexagonal, flat elongated, and truncated triangular shapes with the average diameter of  $24.38 \pm 6.02$  nm were detected. Considering from Figure 4.15(A), the hexagonal shapes found in the representative TEM image were corner truncated, which their edges were nearly etched and transformed to flat rounded shape eventually. This phenomenon occurred since there were no enough effective capping agent to prevent etching of their protruding edges. As a result, the flat elongated AgNPs were grown from round plates and found in this reaction. For the reaction using A30 DNA, only spherical ( $26.53 \pm 6.96$  nm) AgNPs were obtained without the presence of non-spherical morphology.

The optimized molar ratio between  $\text{AgNO}_3$  and plasmid DNA used in this work was 0.2 mM:0.4 nM. In contrast, this molar ratio did not work for the short A30 and C30 DNA. The molar ratio must be increased to 0.2 mM: 1.6 nM in order to obtain non-spherical AgNPs. Thus, DNA length, molar ratio of  $\text{AgNO}_3$  and DNA, and reaction time affected the light-induced shape transformation of spherical Ag seeds into non-spherical shapes. Moreover, the morphologies and colloidal color of C30-capped AgNPs were similar to those of plasmid-capped AgNPs. It is likely that the nanoplate (hexagonal and triangle) morphologies of DNA-capped AgNPs attributed to the interaction of cytosine to certain silver planes.

**Table 4.1** Comparison of optimized synthesis condition and morphologies of the synthesized AgNPs.

AgNPs	[AgNO <sub>3</sub> ]:[DNA]	Light exposure time	Shape			
			Spherical	Hexagonal	truncated triangle	Flat elongate
Plasmid-capped AgNPs	0.2 mM: 0.4 nM	24	√	√	√	X
A30-capped AgNPs	0.2 mM: 1.6 nM	48	√	X	X	X
C30-capped AgNPs	0.2 mM: 1.6 nM	48	√	√	√	√

### 4.3.2 Antibacterial activity

The A30-capped and C30-capped AgNPs exhibited the lower antibacterial activity comparing to that of the plasmid-capped AgNPs. As seen in Table 4.2, the MIC values of A30-capped and C30-capped AgNPs against both bacteria were 4 times higher than that of the plasmid-capped AgNPs. Similarly, the MBC values of A30-capped and C30-capped AgNPs against *E. coli* and *S. aureus* were higher than that of the plasmid-capped AgNPs; 8 times and 4 times higher, respectively. During incubation at 37 °C, some A30-capped and C30-capped AgNPs were aggregated at the bottom of the 96-well plates as seen from the black precipitates. Therefore, the lower antibacterial efficacy of these two synthesized AgNPs possibly resulted from the lesser stability of the formed nanoparticles. Since the length of oligonucleotides used in this work was approximately 260 times shorter than pGADT7-AD, the stability of AgNPs stabilized by these short DNA was lower than the nanoparticles stabilized by long DNA (Tejamaya et al., 2012).

**Table 4.2** Comparison of the MIC and MBC values of the synthesized AgNPs.

Sample	MIC values ( $\mu\text{g/ml}$ )		MBC values ( $\mu\text{g/ml}$ )	
	<i>E. coli</i>	<i>S. aureus</i>	<i>E. coli</i>	<i>S. aureus</i>
Plasmid-capped AgNPs	40	40	40	80
dA-capped AgNPs	160	160	320	320
dC-capped AgNPs	160	160	320	320

### 4.3.3 Antioxidant activity

The antioxidant activity of the synthesized AgNPs was reported in the maximum percentage of DPPH scavenging activity and IC<sub>50</sub> values as shown in Table 4.3. In contrast to antibacterial activity, the antioxidant activities of all synthesized AgNPs were not significantly different ( $P\text{-value}>0.05$ ). The IC<sub>50</sub> values of the plasmid-capped, A30-capped, and C30-capped AgNPs were similar at  $7.34 \pm 0.76$ ,  $6.78 \pm 0.83$ , and  $6.98 \pm 0.46 \mu\text{g/ml}$ , respectively. The maximum percentage of DPPH scavenging activities of all synthesized AgNPs were also insignificantly different. Based on the results of this work, the antioxidant activity of DNA-capped AgNPs did not depend on their size and shape.

**Table 4.3** The maximum percentage of DPPH scavenging activity and IC<sub>50</sub> values of the synthesized AgNPs.

Sample	Maximum % DPPH scavenging activity	IC <sub>50</sub> value ( $\mu\text{g/ml}$ )
Ascorbic acid (positive control)	$94.28 \pm 0.23^b$	$4.41 \pm 0.13^b$
plasmid-capped AgNPs	$45.17 \pm 8.07^a$	$7.34 \pm 0.76^a$
dA-capped AgNPs	$49.17 \pm 3.38^a$	$6.78 \pm 0.83^a$
dC-capped AgNPs	$50.28 \pm 1.46^a$	$6.98 \pm 0.46^a$

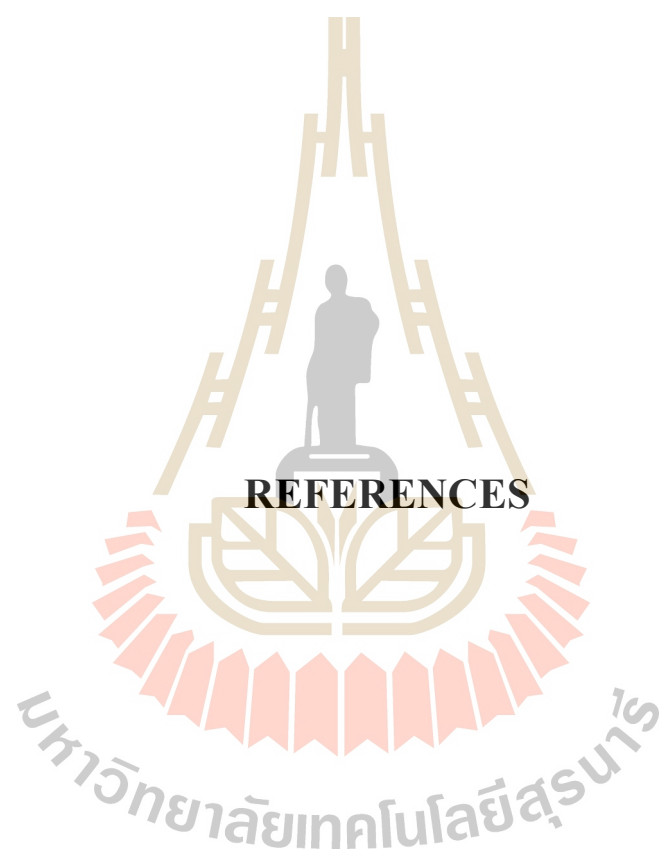
## CHAPTER V

### CONCLUSION

This work demonstrated the photo-induced shape conversion of AgNPs using the 8.0-kb plasmid DNA (pGADT7-AD), oligo dA (30 mers), and oligo dC (30 mers) to assist the formation of non-spherical AgNPs. The DNA content, DNA length, molar ratio of AgNO<sub>3</sub> and DNA, wavelength of LEDs, and irradiation time were the key factors to convert the seeded AgNPs into anisotropic shapes. Among blue, red, and red LEDs, only blue LEDs of 460 nm is the potential light source for the shape-transformation of AgNPs. The length of DNA affects the light-induced shape transformation of AgNPs in terms of optimized synthesis condition, the obtained morphologies, and stability of the synthesized AgNPs. The long DNA (pGADT7-AD) could induce the conversion of small spherical AgNPs to non-spherical shape at 4 pmole, in which spherical (66%), hexagonal (26%), and corner-truncated triangle (8%) shapes were obtained. On the other hands, the short C30 DNA could assist this process when the DNA content was 16 pmole. From this condition, the green colloidal AgNPs consisting of spherical, truncated hexagonal, flat elongated, and truncated triangular shapes were observed. However, the short A30 DNA could produce only spherical AgNPs and appeared as yellow colloidal solution. Moreover, the shape transformation mediated by plasmid DNA could complete within 24 h of light irradiation, whereas the short DNA need the longer exposure time at 48 h to drive this process. The identity of all synthesized AgNPs was confirmed by SAED-TEM,

HR-TEM, and XRD analyses, which suggested their polycrystalline in nature and purity. All synthesized AgNPs exhibited the antioxidant and antibacterial activities in a dose-response manner. Among them, the plasmid-capped AgNPs exhibited the greatest antibacterial activity against both *E. coli* and *S. aureus*, suggesting their potential applications as an antibacterial agent.





**REFERENCES**

## REFERENCES

- Agnihotri, S., and Mukherji, S. (2014). Size-controlled silver nanoparticles synthesized over the range 5–100 nm using the same protocol and their antibacterial efficacy. **RSC Adv.** 4(8): 3974-3983.
- Ahmed, Q., Gupta, N., Kumar, A., and Nimesh, S. (2017). Antibacterial efficacy of silver nanoparticles synthesized employing *Terminalia arjuna* bark extract. **Artif Cells Nanomed Biotechnol.** 45(6): 1192-1200.
- Ajayi, E., and Afolayan, A. (2017). Green synthesis, characterization and biological activities of silver nanoparticles from alkalized *Cymbopogon citratus* Stapf. **Adv Nat Sci Nanosci Nanotechnol.** 8(1): 1-7.
- Ajitha, B., Reddy, Y. A. K., Reddy, P. S., Jeon, H.-J., and Ahn, C. W. (2016). Role of capping agents in controlling silver nanoparticles size, antibacterial activity and potential application as optical hydrogen peroxide sensor. **RSC Adv.** 6(42): 36171-36179.
- Al-Ghamdi, H. S., and Mahmoud, W. E. (2014). Synthesis of self-assembly plasmonic silver nanoparticles with tunable luminescence color. **J Lumin.** 145: 880-883.
- Amany, A., El-Rab, S. F. G., and Gad, F. (2012). Effect of reducing and protecting agents on size of silver nanoparticles and their anti-bacterial activity. **Der Pharma Chemica.** 4(1): 53-65.
- Anandalakshmi, K., Venugobal, J., and Ramasamy, V. (2016). Characterization of silver nanoparticles by green synthesis method using *Pedaliium murex* leaf extract and their antibacterial activity. **Appl Nanosci.** 6(3): 399-408.



- Beyene, H. D., Werkneh, A. A., Bezabh, H. K., and Ambaye, T. G. (2017). Synthesis paradigm and applications of silver nanoparticles (AgNPs), a review. **SM&T**. 13: 18-23.
- Boesenberg-Smith, K. A., Pessarakli, M. M., and Wolk, D. M. (2012). Assessment of DNA yield and purity: an overlooked detail of PCR troubleshooting. **Clin Microbiol Newsl**. 34(1): 1-6.
- Cardoso-Avila, P., Pichardo-Molina, J., Krishna, C. M., and Castro-Beltran, R. (2015). Photochemical transformation of silver nanoparticles by combining blue and green irradiation. **J Nanoparticle Res**. 17(3): 160.
- Cathcart, N., Frank, A. J., and Kitaev, V. (2009). Silver nanoparticles with planar twinned defects: effect of halides for precise tuning of plasmon resonance maxima from 400 to > 900 nm. **Chem Comm**. (46): 7170-7172.
- Chumpol, J., and Siri, S. (2017). Simple green production of silver nanoparticles facilitated by bacterial genomic DNA and their antibacterial activity. **Artif Cells Nanomed Biotechnol**. 46(3): 1-7.
- Dixit, K., and Ali, R. (2001). Antigen binding characteristics of antibodies induced against nitric oxide modified plasmid DNA. **Biochim Biophys Acta**. 1528(1): 1-8.
- Farkhari, N., Abbasian, S., Moshaii, A., and Nikkhah, M. (2016). Mechanism of adsorption of single and double stranded DNA on gold and silver nanoparticles: investigating some important parameters in bio-sensing applications. **Colloids Surf B Biointerfaces**. 148: 657-664.

- Guzman, M., Dille, J., and Godet, S. (2012). Synthesis and antibacterial activity of silver nanoparticles against gram-positive and gram-negative bacteria. **Nanomed Nanotechnol.** 8(1): 37-45.
- Haghi, A., Zachariah, A. K., and Kalariakkal, N. (2013a). **Nanomaterials: Synthesis, Characterization, and Applications.** Boca Raton, FL: CRC Press.
- Haghi, A., Zachariah, A. K., and Kalariakkal, N. (2013b). **Nanomaterials: Synthesis, Characterization, and Applications.** Boca Raton, FL: CRC Press.
- Hong, X., Wen, J., Xiong, X., and Hu, Y. (2016). Shape effect on the antibacterial activity of silver nanoparticles synthesized via a microwave-assisted method. **Environ Sci Pollut Res.** 23(5): 4489-4497.
- Huo, Y., Singh, P., Kim, Y. J., Soshnikova, V., Kang, J., Markus, J., Ahn, S., Castro-Aceituno, V., Mathiyalagan, R., and Chokkalingam, M. (2017). Biological synthesis of gold and silver chloride nanoparticles by *glycyrrhiza uralensis* and in vitro applications. **Artif Cells Nanomed Biotechnol.** 46(2): 1-13.
- Janthima, R., Khamhaengpol, A., and Siri, S. (2017). Egg extract of apple snail for eco-friendly synthesis of silver nanoparticles and their antibacterial activity. **Artif Cells Nanomed Biotechnol.** 46(2): 361-367.
- Jin, R., Cao, Y., Mirkin, C. A., Kelly, K., Schatz, G. C., and Zheng, J. (2001). Photoinduced conversion of silver nanospheres to nanoprisms. **Science.** 294(5548): 1901-1903.
- Khamhaengpol, A., and Siri, S. (2016). Fluorescent light mediated a green synthesis of silver nanoparticles using the protein extract of weaver ant larvae. **J Photochem Photobiol B.** 163: 337-344.

- Khan, F. U., Chen, Y., Khan, N. U., Khan, Z. U. H., Khan, A. U., Ahmad, A., Tahir, K., Wang, L., Khan, M. R., and Wan, P. (2016). Antioxidant and catalytic applications of silver nanoparticles using *Dimocarpus longan* seed extract as a reducing and stabilizing agent. **J Photochem Photobiol B Biol.** 164: 344-351.
- Kharat, S. N., and Mendhulkar, V. D. (2016). Synthesis, characterization and studies on antioxidant activity of silver nanoparticles using *Elephantopus scaber* leaf extract. **Mater Sci Eng C.** 62: 719-724.
- Krajczewski, J., Joubert, V., and Kudelski, A. (2014). Light-induced transformation of citrate-stabilized silver nanoparticles: photochemical method of increase of SERS activity of silver colloids. **Colloids Surf A.** 456: 41-48.
- Krajczewski, J., Kołataj, K., and Kudelski, A. (2015). Light-induced growth of various silver seed nanoparticles: A simple method of synthesis of different silver colloidal SERS substrates. **Chem Phys Lett.** 625: 84-90.
- Krishnan, R., Arumugam, V., and Vasaviah, S. K. (2015). The MIC and MBC of Silver Nanoparticles against *Enterococcus faecalis*-A Facultative Anaerobe. **J Nanomed Nanotechnol.** 6(3): 285-288.
- Lee, G. P., Shi, Y., Lavoie, E., Daeneke, T., Reineck, P., Cappel, U. B., Huang, D. M., and Bach, U. (2013). Light-driven transformation processes of anisotropic silver nanoparticles. **ACS nano.** 7(7): 5911-5921.
- Lee, J.-H., Lim, J.-M., Velmurugan, P., Park, Y.-J., Park, Y.-J., Bang, K.-S., and Oh, B.-T. (2016). Photobiologic-mediated fabrication of silver nanoparticles with antibacterial activity. **J Photochem Photobiol B Biol.** 162: 93-99.

- Levard, C., Hotze, E. M., Lowry, G. V., and Brown Jr, G. E. (2012). Environmental transformations of silver nanoparticles: impact on stability and toxicity. **Environ Sci Technol.** 46(13): 6900-6914.
- Li, J., Zhu, Z., Liu, F., Zhu, B., Ma, Y., Yan, J., Lin, B., Ke, G., Liu, R., and Zhou, L. (2016). DNA-Mediated Morphological Control of Silver Nanoparticles. **Small.** 12(39): 5449-5487.
- Liang, X., Kuhn, H., and Frank-Kamenetskii, M. D. (2006). Monitoring single-stranded DNA secondary structure formation by determining the topological state of DNA catenanes. **Biophys J.** 90(8): 2877-2889.
- Liu, M., Leng, M., Yu, C., Wang, X., and Wang, C. (2010). Selective synthesis of hexagonal Ag nanoplates in a solution-phase chemical reduction process. **Nano Res.** 3(12): 843-851.
- Lu, Y.-C., and Chou, K.-S. (2008). A simple and effective route for the synthesis of nano-silver colloidal dispersions. **J Chin Inst Eng.** 39(6): 673-678.
- Mansouri, S. S., and Ghader, S. (2009). Experimental study on effect of different parameters on size and shape of triangular silver nanoparticles prepared by a simple and rapid method in aqueous solution. **Arab J Chem.** 2(1): 47-53.
- Morones, J. R., Elechiguerra, J. L., Camacho, A., Holt, K., Kouri, J. B., Ramírez, J. T., and Yacaman, M. J. (2005). The bactericidal effect of silver nanoparticles. **Nanotechnology.** 16(10): 2346-2353.
- Moteriya, P., and Chanda, S. (2016). Synthesis and characterization of silver nanoparticles using *Caesalpinia pulcherrima* flower extract and assessment of their in vitro antimicrobial, antioxidant, cytotoxic, and genotoxic activities. **Artif Cells Nanomed Biotechnol.** 45(8):1556-1567.

- Mulfinger, L., Solomon, S. D., Bahadory, M., Jeyarajasingam, A. V., Rutkowsky, S. A., and Boritz, C. (2007a). Synthesis and study of silver nanoparticles. **J Chem Educ.** 84(2): 322.
- Mulfinger, L., Solomon, S. D., Bahadory, M., Jeyarajasingam, A. V., Rutkowsky, S. A., and Boritz, C. (2007b). Synthesis and study of silver nanoparticles. **J Chem Educ.** 84(2): 322-325.
- Nateghi, M. R., and Hajimirzababa, H. (2014). Effect of silver nanoparticles morphologies on antimicrobial properties of cotton fabrics. **J Text I.** 105(8): 806-813.
- Nithyaja, B., Misha, H., and Nampoore, V. (2012). Synthesis of silver nanoparticles in DNA template and its influence on nonlinear optical properties. **J Nanosci Nanotechnol.** 2(4): 99-103.
- Ortega-Arroyo, L., Martin-Martinez, E. S., Aguilar-Mendez, M. A., Cruz-Orea, A., Hernandez-Pérez, I., and Glorieux, C. (2013). Green synthesis method of silver nanoparticles using starch as capping agent applied the methodology of surface response. **Starch-Stärke.** 65(9-10): 814-821.
- Osibe, D. A., Chiejina, N. V., Ogawa, K., and Aoyagi, H. (2017). Stable antibacterial silver nanoparticles produced with seed-derived callus extract of *Catharanthus roseus*. **Artif Cells Nanomed Biotechnol:** 1-8.
- Pacioni, N. L., Borsarelli, C. D., Rey, V., and Veglia, A. V. (2015). Synthetic Routes for the Preparation of Silver Nanoparticles. In: **Silver Nanoparticle Applications.** New York City, NY: Springer, pp. 13-46
- Pardha-Saradhi, P., Yamal, G., Peddisetty, T., Sharmila, P., Nagar, S., Singh, J., Nagarajan, R., and Rao, K. S. (2014). Reducing strength prevailing at root

surface of plants promotes reduction of Ag<sup>+</sup> and generation of Ag<sub>0</sub>/Ag<sub>2</sub>O nanoparticles exogenously in aqueous phase. **Plos one**. 9(9): 1-13.

Park, Y. M., Lee, B. G., Weon, J.-I., and Kim, M. H. (2016). One-step synthesis of silver nanoplates with high aspect ratios: using coordination of silver ions to enhance lateral growth. **RSC Adv**. 6(98): 95768-95773.

Patra, J. K., Das, G., and Baek, K.-H. (2016). Phyto-mediated biosynthesis of silver nanoparticles using the rind extract of watermelon (*Citrullus lanatus*) under photo-catalyzed condition and investigation of its antibacterial, anticandidal and antioxidant efficacy. **J Photochem Photobiol B Biol**. 161: 200-210.

Pietrobon, B., and Kitaev, V. (2008). Photochemical synthesis of monodisperse size-controlled silver decahedral nanoparticles and their remarkable optical properties. **Chem Mater**. 20(16): 5186-5190.

Raza, M. A., Kanwal, Z., Rauf, A., Sabri, A. N., Riaz, S., and Naseem, S. (2016). Size- and shape-dependent antibacterial studies of silver nanoparticles synthesized by wet chemical routes. **Nanomaterials**. 6(4): 74.

Rivero, P. J., Goicoechea, J., Urrutia, A., and Arregui, F. J. (2013). Effect of both protective and reducing agents in the synthesis of multicolor silver nanoparticles. **Nanoscale Res Lett**. 8(1): 101.

Roy, E., Patra, S., Saha, S., Madhuri, R., and Sharma, P. K. (2015). Shape-specific silver nanoparticles prepared by microwave-assisted green synthesis using pomegranate juice for bacterial inactivation and removal. **RSC Adv**. 5(116): 95433-95442.

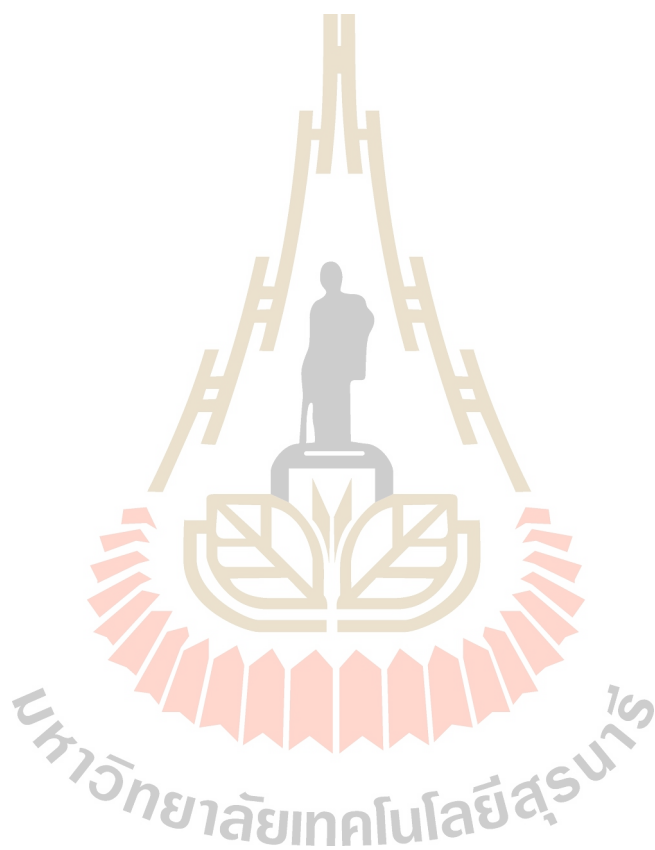
- Saade, J., and de Araújo, C. B. (2014). Synthesis of silver nanoprisms: a photochemical approach using light emission diodes. **Mater Chem Phys.** 148(3): 1184-1193.
- Sambrook, J., Fritsch, E. F., and Maniatis, T. (1989). **Molecular cloning: a laboratory manual.** Cold Spring Harbor, NY: Cold spring harbor laboratory press.
- Singh, H., Du, J., Singh, P., and Yi, T. H. (2017). Ecofriendly synthesis of silver and gold nanoparticles by *Euphrasia officinalis* leaf extract and its biomedical applications. **Artif Cells Nanomed Biotechnol.** 46(6):1163-1170.
- Stamplecoskie, K. G., and Scaiano, J. C. (2010). Light emitting diode irradiation can control the morphology and optical properties of silver nanoparticles. **J Am Chem Soc.** 132(6): 1825-1827.
- Szeremeta, J., Nyk, M., and Samoc, M. (2014). Photocurrent enhancement in polythiophene doped with silver nanoparticles. **Opt Mater.** 37: 688-694.
- Tan, L. H., Xing, H., and Lu, Y. (2014). DNA as a powerful tool for morphology control, spatial positioning, and dynamic assembly of nanoparticles. **Acc Chem Res.** 47(6): 1881-1890.
- Tang, B., Sun, L., Li, J., Zhang, M., and Wang, X. (2015). Sunlight-driven synthesis of anisotropic silver nanoparticles. **Chem Eng J.** 260: 99-106.
- Tao, A. R., Habas, S., and Yang, P. (2008). Shape control of colloidal metal nanocrystals. **Small.** 4(3): 310-325.
- Tejamaya, M., Römer, I., Merrifield, R. C., and Lead, J. R. (2012). Stability of citrate, PVP, and PEG coated silver nanoparticles in ecotoxicology media. **Environ Sci Technol.** 46(13): 7011-7017.

- Troupis, A., Triantis, T., Hiskia, A., and Papaconstantinou, E. (2008). Rate-Redox-Controlled Size-Selective Synthesis of Silver Nanoparticles Using Polyoxometalates. **Eur J Inorg Chem.** 2008(36): 5579-5586.
- Upadhyay, L. S. B., and Verma, N. (2015). Recent developments and applications in plant-extract mediated synthesis of silver nanoparticles. **Anal Lett.** 48(17): 2676-2692.
- Van Dong, P., Ha, C. H., and Kasbohm, J. (2012). Chemical synthesis and antibacterial activity of novel-shaped silver nanoparticles. **Nano Lett.** 2(1): 1-9.
- Verma, S., Rao, B. T., Srivastava, A., Srivastava, D., Kaul, R., and Singh, B. (2017). A facile synthesis of broad plasmon wavelength tunable silver nanoparticles in citrate aqueous solutions by laser ablation and light irradiation. **Colloids Surf A.** 527: 23-33.
- Wang, Z., Tang, L., Tan, L. H., Li, J., and Lu, Y. (2012). Discovery of the DNA “genetic code” for abiological gold nanoparticle morphologies. **Angew Chem.** 51(36): 9078-9082.
- Wang, Z., Zhang, J., Ekman, J. M., Kenis, P. J., and Lu, Y. (2010). DNA-mediated control of metal nanoparticle shape: one-pot synthesis and cellular uptake of highly stable and functional gold nanoflowers. **Nano Lett.** 10(5): 1886-1891.
- Wiegand, I., Hilpert, K., and Hancock, R. E. (2008). Agar and broth dilution methods to determine the minimal inhibitory concentration (MIC) of antimicrobial substances. **Nat Protoc.** 3(2): 163-175.
- Wiley, B., Sun, Y., Mayers, B., and Xia, Y. (2005). Shape-controlled synthesis of metal nanostructures: the case of silver. **Chem Eur J.** 11(2): 454-463.



- Xia, Y., Xia, X., and Peng, H.-C. (2015). Shape-controlled synthesis of colloidal metal nanocrystals: thermodynamic versus kinetic products. **J Am Chem Soc.** 137(25): 7947-7966.
- Xia, Y., Xiong, Y., Lim, B., and Skrabalak, S. E. (2009). Shape-controlled synthesis of metal nanocrystals: Simple chemistry meets complex physics? **Angew Chem.** 48(1): 60-103.
- Yi, Z., Xu, X., Wu, X., Chen, C., Li, X., Luo, B., Luo, J., Jiang, X., Wu, W., and Yi, Y. (2013). Silver nanoplates: controlled preparation, self-assembly, and applications in surface-enhanced Raman scattering. **Appl Phys A.** 110(2): 335-342.
- Yu, P., Huang, J., and Tang, J. (2011). Observation of coalescence process of silver nanospheres during shape transformation to nanoprisms. **Nanoscale Res Lett.** 6(1): 46-53.
- Zeng, J., Zheng, Y., Rycenga, M., Tao, J., Li, Z.-Y., Zhang, Q., Zhu, Y., and Xia, Y. (2010). Controlling the shapes of silver nanocrystals with different capping agents. **J Am Chem Soc.** 132(25): 8552-8553.
- Zhang, X., Yu, M., Liu, J., and Li, S. (2011). Fabrication and characterization of Ag nanoparticles based on plasmid DNA as templates. **Mater Lett.** 65(4): 719-721.
- Zheng, X., Xu, W., Corredor, C., Xu, S., An, J., Zhao, B., and Lombardi, J. R. (2007). Laser-induced growth of monodisperse silver nanoparticles with tunable surface plasmon resonance properties and a wavelength self-limiting effect. **J Phys Chem Lett.** 111(41): 14962-14967.

Zhu, L., Wei, B., Xu, L., Lü, Z., Zhang, H., Gao, H., and Che, J. (2012). Ag<sub>2</sub>O–Bi<sub>2</sub>O<sub>3</sub> composites: synthesis, characterization and high efficient photocatalytic activities. **Cryst EngComm**. 14(18): 5705-5709.



## CURRICULUM VITAE

**Name** Navaporn Sritong

**Date of birth** January 12, 1994

**Place of birth** Nakhon Ratchasima, Thailand

### Education

2016 – 2018

**MSc in Environmental Biology**

Suranaree University of Technology, Nakhon Ratchasima,  
Thailand

2012 – 2016

**BSc in Biology (Honors Program, First Class Degree Honor)**

Suranaree University of Technology, Nakhon Ratchasima,  
Thailand

### Publication

Sritong, N., Chumsook, S., and Siri, S. (2018). Light emitting diode irradiation induced shape conversion of DNA-capped silver nanoparticles and their antioxidant and antibacterial activities. **Artif Cells Nanomed Biotechnol.** 46: 1-9